J Mater Sci: Mater Electron **(2024) 35:996**

Synthesis and characterization of $BaIrO_3$-doped YBCO superconducting thin films via TFA-MOD technique

Murat Bektas[1], Isil Birlik[1], and Erdal Celik[2,3,*]

[1] *Department of Metallurgical and Materials Engineering, Faculty of Engineering, Dokuz Eylul University, Buca, Izmir, Turkey*
[2] *Department of Mechanical Engineering, Faculty of Mechanical Engineering, Istanbul Technical University, Beyoglu, Istanbul, Turkey*
[3] *Turkish Aerospace Industries Inc. (TAI), R&D and Technology Directorate, Kahramankazan, Ankara, Turkey*

Received: 9 February 2024
Accepted: 15 April 2024
Published online: 22 May 2024

© The Author(s), 2024

ABSTRACT

High-temperature superconducting materials (HTS) are characterized by remarkably high critical current density (J_c) values when exposed to low temperatures and magnetic fields. In the realm of such investigations, various crystalline imperfections, including finely dispersed non-superconducting phases, dislocations, vacancies, grain boundaries, twin boundaries, antiphase boundaries, and insulating regions within grain boundaries, have been recognized as potential sources of pinning centers. However, it is essential to acknowledge that J_c values experience a rapid decline as the temperature rises in the presence of a magnetic field. The primary contributing factors to this decline are attributed to the intrinsic crystalline anisotropy of HTS materials and the thermal fluctuations that prevail at elevated temperatures. Nevertheless, a noteworthy factor in the diminishment of J_c values is the scarcity of efficacious pinning centers. In response to these challenges, a pioneering technology has emerged, revolving around nanostructure engineering for the deliberate creation of artificial pinning centers within HTS materials. In alignment with this approach, the present study endeavors to augment the critical current density and enhance the flux pinning properties of $YBa_2Cu_3O_{6.56}$ (YBCO) superconducting films. This augmentation is achieved through the integration of $BaIrO_3$ (BIO) perovskite nanodots, nanorods, or nanoparticles as strategically positioned pinning centers. The films are deposited on a $SrTiO_3$ (STO) substrate employing the Trifluoroacetate Metal–Organic Deposition (TFA-MOD) technique. This research initiative seeks to contribute to the advancement of knowledge regarding the controlled manipulation of artificial pinning centers in HTS materials, particularly focusing on YBCO thin films, with the ultimate goal of enhancing their performance under the influence of elevated magnetic fields.

Address correspondence to E-mail: erdal.celik@tai.com.tr; erdalcelik@itu.edu.tr; ercelik2000@gmail.com

https://doi.org/10.1007/s10854-024-12607-3

1 Introduction

Yttrium Barium Copper Oxide ($YBa_2Cu_3O_{6.56}$, YBCO) has garnered significant attention as one of the preeminent high-temperature superconductors due to its inherent potential and alluring attributes for a spectrum of practical applications. This multifaceted superconducting material has been extensively investigated for its utilization in diverse technological domains, encompassing but not limited to energy storage systems, current limiters, and magnetic bearings. Notably, YBCO exhibits its exceptional superconducting properties at temperatures surpassing the critical threshold of liquid nitrogen (77 K), thereby rendering it exceptionally appealing for these intended applications [1, 2].

In the preparation of buffer and YBCO layers, a spectrum of deposition techniques is employed, encompassing both physical and chemical methods [3]. These methodologies, as elucidated by Knoth et al. [4], encompass pulsed laser deposition (PLD), sputtering, thermal and electron-beam evaporation, as well as chemical deposition techniques such as chemical vapor deposition and chemical solution deposition (CSD). Within the realm of chemical solution deposition (CSD), the film fabrication process can be categorized into two primary approaches: the sol–gel process and metal organic deposition (MOD) techniques [5]. The sol–gel technique represents a low-temperature synthesis method for material production, yielding products that are either entirely composed of inorganic constituents or a combination of inorganic and organic components. This process is esteemed for its ability to generate thin bond coatings that facilitate robust adhesion between the metallic substrate and the top coat, resulting in high homogeneity and purity of the resultant materials [4, 6]. A particularly promising technique within the domain of metal organic deposition is the Trifluoroacetate Metal–Organic Deposition (TFA-MOD) method. This approach, as outlined by Nakaoka et al. [7], holds significant potential for the cost-effective fabrication of extended-length YBCO tapes with exceptional performance characteristics. Notably, TFA-MOD leverages trifluoroacetates, which are yttrium, barium, and copper salts, as the key starting solution for the deposition process, thus contributing to its efficacy and affordability in producing high-quality YBCO materials.

Within the context of TFA-MOD, a noteworthy consideration pertains to the occurrence of chemical reactions during the calcination and firing stages of the process, leading to the generation of water vapor and hydrogen fluoride (HF) gas. These chemical byproducts can engender adverse interactions with the substrate and buffer layers, resulting in detrimental consequences for the superconducting properties of the final YBCO film. Consequently, the selection of a judiciously chosen buffer layer emerges as a pivotal requirement in the TFA-MOD methodology. It is discerned that alkaline and alkaline earth oxides, specifically those elements belonging to groups IA and IIA in the periodic table, exhibit a propensity to react with HF gas during the firing process [8, 9]. For illustrative purposes, while YBCO films can be successfully deposited onto Lanthanum Aluminate ($LaAlO_3$, LAO) or Strontium Titanate ($SrTiO_3$, STO) substrates, they encounter substantial hindrances when attempted on a Magnesium Oxide (MgO) substrate, as elucidated by Araki and Hirabayashi [10]. This underscores the paramount importance of substrate material choice in mitigating the detrimental impact of HF gas-induced reactions and preserving the superconducting integrity of the final YBCO film.

The quest for achieving a heightened critical current density (J_c), particularly in the presence of elevated applied magnetic fields, constitutes a paramount objective in the realm of superconducting materials. To augment the value of J_c, it becomes imperative to fortify the anchoring of the flux line lattice through the strategic introduction of diverse crystal imperfections. Additionally, there is a requisite for amplifying the pinning force density, which plays a pivotal role in resisting the movement of flux lines. This enhanced pinning efficacy serves as a critical means to bolster the overall superconducting performance.

Recent endeavors within the YBCO system have been directed toward optimizing pinning efficiency. These efforts encompass the implementation of chemical doping strategies and the deliberate introduction of non-superconducting secondary phases. These measures, as investigated by Jha and Khare [1], aim to fortify the pinning mechanisms within the YBCO framework, thereby fostering higher critical current densities and, consequently, improving the superconducting characteristics, particularly in the presence of challenging magnetic field conditions.

Numerous research groups have extensively explored the mechanisms underlying the formation of efficacious pinning centers within YBCO layers, primarily employing the PLD technique. Their primary

emphasis has revolved around augmenting intragrain pinning, achieved through intricate structural modifications in composite rare earth films or the incorporation of nanoscale inclusions such as Barium Iridate ($BaIrO_3$, BIO) [11], Barium Hafnate ($BaHfO_3$, BHO) [12], Yttrium Barium Cuprate (Y_2BaCuO_5) [13], Barium Zirconate ($BaZrO_3$, BZO), and Yttrium Oxide (Y_2O_3) [14]. These research endeavors have yielded highly encouraging outcomes, including substantial enhancements in critical current densities and the expansion of irreversibility fields [12].

The primary research focus has been on refining the efficacy of flux line pinning within High-Temperature Superconductor (HTS) films, as elucidated by Aytug et al. [15]. Among the various options, the integration of BZO nanoparticles into YBCO thin films has gained prominence for its ability to impede vortex motion at elevated magnetic fields. Birlik et al. [16] executed investigations encompassing both undoped and BZO-doped YBCO thin films using the CSD method. It is worth noting, however, that there exists a paucity of scholarly inquiry concerning the utilization of BIO as artificial pinning centers in this context. Further research in this area is warranted to elucidate their potential contributions to enhancing the pinning properties of YBCO thin films.

Amid the diverse array of physical and chemical techniques employed for the fabrication of YBCO superconducting films, the MOD method has emerged as a notably advantageous approach, owing to its inherent versatility and cost-effectiveness, as corroborated by the findings of Roma et al. [17]. YBCO, recognized as one of the most extensively researched high-temperature superconductors, has garnered substantial attention due to its promising and appealing attributes for potential applications, particularly above the critical temperature of liquid nitrogen (77 K). In the context of practical utility, the attainment of a robust J_c, even under elevated applied magnetic fields, remains a paramount objective. Enhancing the value of J_c necessitates the effective immobilization of the flux line lattice through the strategic introduction of crystal imperfections, thereby increasing the pinning force density. It is worth emphasizing that the pinning of the flux line lattice in high-temperature superconductors is generally feeble, particularly at elevated temperatures and in the presence of strong magnetic fields. Consequently, augmenting the flux pinning strength mandates the deliberate incorporation of artificial pinning centers within the superconducting material, distinct from naturally occurring pinning sites. In the pursuit of enhancing the J_c of YBCO thin films, a pioneering methodology has been developed, involving the domain of nanostructure engineering to fabricate artificial pinning centers within HTS materials [3, 4, 18, 19]. Thus, the primary objective of the present investigation resides in augmenting the flux pinning properties of YBCO superconducting films through the integration of BIO perovskite nanoparticles, utilizing the TFA-MOD technique. This research endeavor aspires to contribute to the advancement of scientific understanding pertaining to the controlled manipulation of artificial pinning centers within HTS materials, with a specific focus on YBCO thin films, potentially paving the way for enhanced performance in the presence of elevated magnetic fields.

Preceding the deposition process, a comprehensive assessment of solution characteristics was conducted to facilitate subsequent steps within the TFA-MOD technique. The rheological properties of the YBCO solutions were systematically examined utilizing a rheometer machine. To ascertain the wetting behavior between the solution and the substrate, contact angle measurements were meticulously carried out. For the purpose of optimizing the TFA-MOD methodology, a multifaceted approach was employed, encompassing thermal, structural, and morphological analyses. The thermal behavior of the gel-like precursor material was evaluated via Differential Thermal Analysis-Thermogravimetry (DTA-TG), while Fourier Transform Infrared Spectroscopy (FTIR) was employed to identify and characterize organic complexes present in the dried powder. X-ray Diffraction (XRD) analysis was conducted to discern the crystalline phases within the YBCO-based thin films. Surface chemistry investigations of both pure and BIO-doped YBCO thin films were carried out employing X-ray Photoelectron Spectroscopy (XPS). The surface topography and morphology of the YBCO films were scrutinized using Scanning Electron Microscopy-Energy Dispersive Spectroscopy (SEM–EDS), and the morphological quality of the thin films was meticulously assessed via Atomic Force Microscopy (AFM). The film thickness was precisely determined employing a surface profilometer. In the realm of electrical properties of the superconducting films, T_c and J_c were rigorously investigated within this experimental framework. The T_c and J_c of both pure and BIO-doped YBCO thin films

were systematically determined, enabling the elucidation of dopant-induced effects, with the aid of a JANIS SHI-4 Series 4.2 K Cryostat.

2 Experimental procedure

2.1 Materials

The (100)-oriented commercial STO single-crystal oxides, procured from CrysTec GmbH Company with dimensions of 10 mm × 10 mm × 1 mm, were employed as substrates for the preparation of superconducting thin films. The meticulous preparation of the STO substrate is a pivotal step in ensuring the success of the deposition process for all subsequent coatings. Consequently, the substrate must exhibit cleanliness, freedom from dust, and an absence of contaminants such as oil, grease, paint, wax, curing compounds, or any substances that could potentially act as bond disruptors. The primary objective is to establish a strong bond between the substrate and the superconducting films, thereby underscoring the significance of rigorous surface preparation of STO substrates. To achieve this, the substrate underwent a thorough cleaning process in an ultrasonic bath employing acetone to eliminate impurities from the sample surface.

For the preparation of YBCO-based thin films, precursor materials including yttrium acetate ($Y(CH_3COO)_3{\cdot}4H_2O$), barium acetate ($Ba(CH_3COO)_2$), and copper acetate ($Cu(CH_3COO)$) were used. These precursor materials were dissolved in distilled water (H_2O), serving as the solvent. Trifluoroacetic acid (CF_3COOH, TFA) was used to synthesize dissolved precursors. The solution's concentration was maintained at 0.25 methanol (CH_3OH) as a diluting solvent. Additionally, iridium (III) pentanedionate ($C_{15}H_{21}IrO_6$) was introduced into the pure YBCO solutions as dopant materials.

2.2 Preparation of solutions

It is crucial to underscore that the synthesis of the MOD precursor solution represents a pivotal facet of the MOD processing methodology for coated conductors. An elaborate flowchart, as depicted in Fig. 1, provides a detailed overview of the sequential steps entailed in the synthesis of this precursor solution, offering a comprehensive understanding of the intricacies involved in this crucial phase of the research endeavor.

The precursor solutions for both pure and BIO-doped YBCO were meticulously formulated through a methodical process. This involved dissolving acetates of the constituent elements, namely Yttrium (Y), Barium (Ba), and Copper (Cu), in distilled water while maintaining a specific cation ratio of 1:2:3. To facilitate the dissolution, an arbitrary quantity of trifluoroacetic acid (TFA) was incorporated into the solution at room temperature, with a standard ratio of 10 ml of TFA for every 25 ml of the final solution. This aqueous solution was subsequently subjected to a refinement process under a vacuum atmosphere, utilizing an evaporator. The primary objective of this step was to eliminate the solvent, resulting in the formation of a glassy blue residue. Nonetheless, it is important to note that this residue retained impurities, such as residual water and acetic acid. The experimental setup employed for the evaporation process is visually depicted in Fig. 2, offering a clear representation of the equipment used to carry out this critical step. Subsequently, the obtained residue was re-dissolved, this time in an ample quantity of methanol, and subjected to another refinement process. This step was designed to eliminate any remaining impurities, resulting in the formation of a glassy blue residue containing methanol. To achieve a consistent solution concentration, the addition of methanol was executed with precise control, effectively standardizing the solution concentration to 0.25 M while adhering to specific ratio guidelines.

The ultimate precursor solution was partitioned into seven discrete portions, each consisting of 3 ml in volume. Within these individual portions, varying amounts of iridium were incorporated by dissolving Ir (III) pentanedionate. The concentrations of iridium dopant were meticulously adjusted to specific levels, including 0, 1, 3, and 5 mol percent (mole %). It is pertinent to note that the introduction of iridium into the precursor solutions engendered observable alterations in their chromatic characteristics, spanning a spectrum from various shades of blue to deep green. These modifications in coloration were contingent upon the particular dopant employed and its corresponding concentration. To facilitate clarity and succinctness, Table 1 succinctly encapsulates the abbreviated nomenclature adopted for both the precursor solutions and the ensuing films generated from these solutions. In this naming convention, "Sol" is employed to denote the precursor solutions,

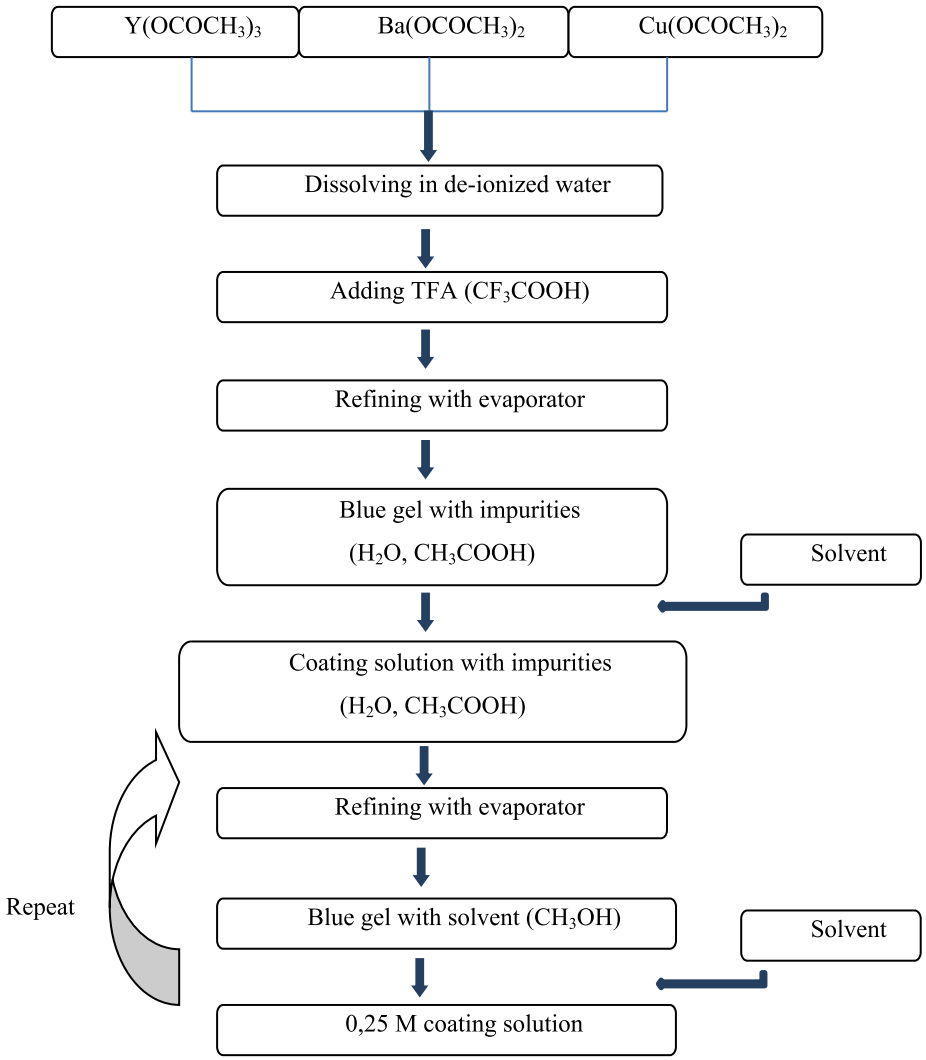


Fig. 1 Schematic illustration of coating solution preparation by yttrium, barium, and copper acetates



Fig. 2 Experimental setup for solution evaporation

while "F" is employed to signify the films that emanated from these precursor solutions. As given in Table 1, abbreviations Sol-0 (undoped), Sol-Ir-1 (1% Ir-doped), Sol-Ir-3 (3% Ir-doped), and Sol-Ir-5 (5% Ir-doped) describe the solutions, while F-0 (YBCO) deposited on STO substrate, F(Ir-1) (1% doped BIO-YBCO), F(Ir-3) (3% doped BIO-YBCO), and F(Ir-5) (5% doped BIO-YBCO) films are specified. Here, varying concentrations of Ir precursor, specifically 0%, 1%, 3%, and 5% molar ratios, were incorporated into YBCO solutions. Subsequently, upon undergoing heat treatment, $BaIrO_3$ (BIO) phases were observed to form. Table 1 provides a comprehensive breakdown of the resultant YBCO films containing 0%, 1%, 3%, and 5% molar ratios of BIO. Consequently, the molarity of the solutions was systematically augmented, leading to corresponding increases in the

Table 1 A brief summary which describes the solutions and the films prepared from these solutions

Name of solution	Type of precursors	Type of solvents	Name of dopant precursors	Doped BIO concentration (mole %)	Name of films on STO substrate
Sol-0	$Y(CH_3COO)_3{\cdot}4H_2O$ $Ba(CH_3COO)_2$ $Cu(CH_3COO)$	H_2O TFA CH_3OH	–	0	F-0 (YBCO)
Sol-Ir-1	$Y(CH_3COO)_3{\cdot}4H_2O$ $Ba(CH_3COO)_2$ $Cu(CH_3COO)$		$C_{15}H_{21}IrO_6$	1	F(Ir-1) (BIO-YBCO)
Sol-Ir-3	$Y(CH_3COO)_3{\cdot}4H_2O$ $Ba(CH_3COO)_2$ $Cu(CH_3COO)$			3	F(Ir-3) (BIO-YBCO)
Sol-Ir-5	$Y(CH_3COO)_3{\cdot}4H_2O$ $Ba(CH_3COO)_2$ $Cu(CH_3COO)$			5	F(Ir-5) (BIO-YBCO)

mole percentages of BIO incorporated within the YBCO films.

2.3 Fabrication of thin films

Uniform gel films were successfully fabricated on single-crystal STO substrates through the meticulous technique of spin coating. During this process, the STO substrate was securely positioned on a turntable within a reduced-pressure environment achieved through the operation of a vacuum pump. It is important to note that the precursor films exhibited a propensity to readily absorb moisture from the ambient environment. Consequently, to mitigate this issue and maintain the integrity of the coating process, all coating procedures were conducted within a controlled dry nitrogen atmosphere. The spin coating procedure entails the methodical application of the coating solution to the substrate. Subsequently, the turntable was set into motion, initiating its rotation. As a result of this controlled rotation, the solvent within the coating solution rapidly underwent vaporization, leading to the formation of a gel film on the surface of the substrate. As a result, in the production of YBCO superconducting thin films, a deliberate strategy was used. This strategy involved the utilization of high rotational speeds, specifically set at 6000 rpm, coupled with an acceleration speed of 6000 rpm per second (6000 rpm s^{-1}). This specific combination of parameters was applied diligently over a duration of 30 s to ensure the attainment of the desired film thickness with enhanced uniformity.

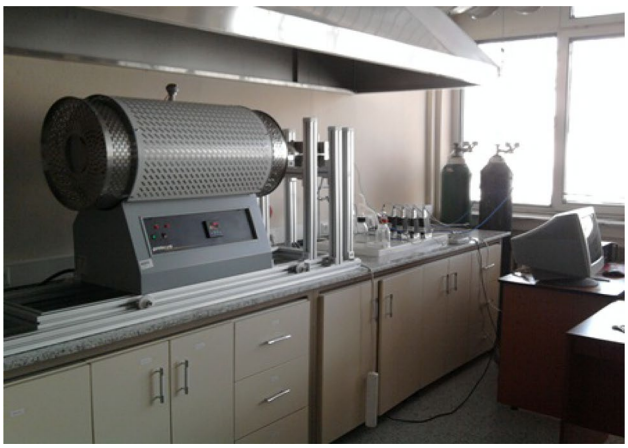


Fig. 3 Atmosphere controlled heat treatment system

The controlled atmosphere heat treatment system employed in this research is depicted in Fig. 3. Precise control of the atmosphere was achieved through the utilization of a computer program. The heat treatment profiles for both pure and BIO-doped YBCO films are illustrated in Fig. 4. It is worth noting that all samples underwent heat treatment in accordance with this prescribed profile. During the initial step, conducted below 60 °C, dry oxygen was introduced to prevent the gel film from absorbing moisture. This precautionary measure was essential as moisture absorption by the gel film could lead to its deterioration. In the subsequent step, which

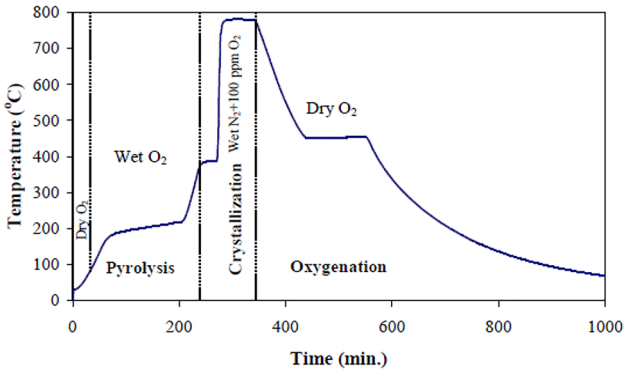


Fig. 4 Heat treatment profile for the production of pure and BIO-doped YBCO films. All films are crystallized at 780 °C and oxygenated at 450 °C [16]

occurred above 60 °C, humidified oxygen (O_2) was introduced into the furnace to inhibit the sublimation of Cu trifluoroacetate. During the pyrolysis step, metal trifluoroacetates within the gel film decomposed, and any deleterious gaseous byproducts were effectively purged. Subsequently, the temperature was elevated to 780 °C for the purpose of crystallization, conducted under humidified nitrogen (N_2) gas containing 100 ppm of O_2. The final superconducting films were ultimately obtained following oxygenation at 450 °C.

2.4 Solution characterization

2.4.1 Rheology measurement

The rheological measurements were meticulously conducted utilizing a Bohlin Instruments CVO 100 Rheometer, employing a 2° conic plate geometry characterized by a diameter of 60 mm and a gap size of 70 µm between the plates. The viscosity values of the precursor solutions were discerned at a controlled temperature of 25 °C, employing a single shear mode, and subsequently under escalating temperature conditions ranging from 25 to 60 °C, all while maintaining a constant frequency of 400 Hertz across all solutions. Furthermore, the gel-point profiles for both pure and BIO-doped precursor solutions were elucidated at 60 °C. The gel point, in this context, is explicated by denoting the temporal instant at which gelation is actualized during the deposition process. This meticulous characterization of rheological properties serves as an essential component in comprehending the intricate dynamics of the precursor solutions, particularly in the context of their gelation behavior and subsequent deposition phenomena.

2.4.2 Contact angle

Contact angle measurements of the precursor solutions were performed to estimate their wettability properties with Contact Angle Meter-CAM 100 (KSV Instruments Ltd., Finland). It is a compact CCD camera-based instrument for measurement of contact angles of liquids on solids. Goniometry involves the observation of a sessile drop of test liquid on a solid substrate. The basic elements of a goniometer include a light source, sample stage, lens, and image capture. Contact angle can be evaluated directly by measuring the angle formed between the solid and the tangent to the drop surface. After measuring the contact angles of the precursor solutions, their values provide film qualities obtained in further processing of MOD-TFA technique.

2.5 Material characterization

2.5.1 Differential thermal analysis-thermogravimetry (DTA-TG)

Thermal behavior of xerogels, which were dried at 100 °C for 3 h in air, was evaluated using DTA/TG machine (DTG-60H Shimadzu) to gain solution evaporation, decomposition, and phase formation and to obtain an optimum heat treatment regime for drying, heat treatment, and annealing processes. Prior to performing DTA-TG measurement of the xerogels, they were weighted as approximately 20 mg and then put into crucible. In these experiments, aluminum oxide (Al_2O_3) powder with 60 µm was used as a reference material. The experiments were conducted under N_2 flow in the temperature range from ambient to 800 °C at a heating rate of 10 °C/min.

2.5.2 Fourier transform infrared spectroscopy (FTIR)

Fourier transform infrared spectroscopy (FTIR) was used for determination of organic compounds/complexes in xerogel powders. For these experiments, pure and BIO-doped precursor solutions were dried at 200 °C for 3 h in air. FTIR (Perkin Elmer)

absorption spectra were measured over the range of 4000–650 cm^{-1} at room temperature in air. In this study, variations of concentration organic components/complexes depending on temperature were determined by Perkin–Elmer Fluka library. By interpreting the FTIR spectra of the xerogel powders, the chemical bonds in a molecule were determined after the measurements.

2.5.3 X-ray diffraction (XRD)

The crystallographic attributes and structural evolution of the synthesized YBCO-based superconducting thin films were meticulously probed through XRD analyses employing a Rigaku D/MAX-2200/PC instrument. The XRD patterns were acquired utilizing CuK_α irradiation with a wavelength (λ) of 0.15418 nm, and the scanning regime encompassed an angular range of $2\theta = 10°$ to 90°. Notably, a step scan approach was employed with a precision step size of 0.02° and a counting time of 1 s/step. This rigorous methodology facilitated the comprehensive examination of the diffraction patterns, affording insights into the crystallographic phases, orientation, and overall structural characteristics of the YBCO thin films. The meticulous control of experimental parameters underscores the precision and reliability of the structural analyses, contributing significantly to the elucidation of the material's crystalline properties and their implications for superconducting behavior.

Structural parameters were obtained from Rietveld refinement using Maud (2.71version) programs. XRD spectra give information about crystal system, crystallographic orientation, lattice parameters, and average crystal size. Equation 1 given below for the texturing coefficient (TC) is used to determine the full orientation.

$$TC = \frac{I_{(hkl)}/I_{0(hkl)}}{(1/N)\left(\sum_N I_{(hkl)}/I_{0(hkl)}\right)}, \quad (1)$$

where $I_{0(hkl)}$ denotes the standard intensity of the (hkl) plane, and $I_{(hkl)}$ denotes the observed intensity of the same plane. For the full orientation, the value of TC should be greater than one [20]. *The interplanar distance d can be calculated by the relationship between the a, b, and c lattice parameters of the crystal structure and (hkl) Miller indices* [20, 21]. The average crystal size can be determined using the Scherrer formula. Mean crystal size is expressed as follows [20, 22]:

$$D = 0.94\lambda/\beta\cos\theta, \quad (2)$$

in which D is the mean crystal size, β is the half-peak width (FWHM) in radians for the respective crystal direction, θ is the Bragg angle, and λ is the wavelength of the X-ray used. The smaller the size of the particles in a material, the wider the peaks in the XRD spectrum. At the same time, the dislocation density can be calculated by using the crystal size value in the crystal. The defect density (δ) gives information about the crystallization of the material. The small value of this value is one of the indicators that the crystallization of the material is good.

$$\delta = 1/D^2. \quad (3)$$

Crystallization quality is closely related to the defect density. According to Eq. 3, a small defect density requires a large crystal size. For a crystal with a large crystal size, it can be interpreted that the half-peak width is narrow. This is proof that crystallization is good [20].

2.5.4 X-ray photoelectron spectroscopy (XPS)

Surface chemistry of pure and BIO-doped YBCO thin films were characterized by means of Thermo Scientific K-Alpha XPS system. Photoemission of electrons was produced using a monochromatic Al K_α X-ray source (1486.6 eV) operated at 150 W. The photoelectrons were allowed to pass through a hemispherical analyzer operated in fixed retardation ratio mode at 11.75 eV of pass energy. This results in an energy resolution of ≤ 0.51 eV. All data were acquired with take-off angle α of the detected electrons ranging from 30° to 70°.

2.5.5 Scanning electron microscopy (SEM)–energy dispersive spectroscopy (EDS)

The surface characteristics, topographical features, and morphological attributes of both pure and BIO-doped YBCO superconducting thin films deposited on STO substrates were systematically investigated through Scanning Electron Microscopy (SEM) using a JEOL JSM 6060 instrument. SEM imaging was conducted at

an accelerated voltage of 20 kV, enabling a comprehensive exploration of the surface microstructure and nanoscale morphology of the thin films. Additionally, Energy Dispersive X-ray Spectroscopy (EDS) analyses were performed concurrently with SEM imaging to provide elemental composition insights.

2.5.6 Atomic force microscope (AFM)

Inasmuch as the AFM is used to more fully characterize the surface morphology and roughness of the superconducting thin films, their two- and three-dimensional surface characteristics were examined with the aid of Nanosurf Easyscan II AFM device.

2.5.7 Film thickness measurement

After obtaining optimum superconducting films, half of the thin films were etched and removed from substrate surface to measure their surface profiles and thicknesses. The step height from substrate to the films is a value for film thickness. The thickness of the films was determined through Ambios Technology XP-2 Surface Profilometer.

2.6 Electrical characterization

In the present work, the electrical properties (T_c, J_c, and B_c) of the superconducting thin film samples were studied by using standard four-probe method.

2.6.1 Critical transition temperature (T_c) measurement

The critical transition temperature of the YBCO-based thin films was determined under cryogenic conditions bearing liquid helium by using Physical Property Measurement System (PPMS) (Inonu University, Scientific and Technological Research Center) under zero magnetic fields. In that a four-probe method is one of the standard and most widely used methods for the measurement of resistivity of superconductors; it was applied to prepare YBCO-based specimens before the transition temperature measurements of the thin films. The Ag paste was utilized to provide four contacts on the superconducting films on STO substrates.

2.6.2 Critical current density (J_c) and critical magnetic field (B_c) measurements

The critical current density (J_c) of the YBCO-based thin films was determined using PPMS. The critical magnetic field (B_c) values of pure and BIO-doped YBCO thin films were measured at 77 K in up to 9 T magnetic field by using the same PPMS device (Inonu University, Scientific and Technological Research Center). All measurements were performed by standard four-probe method and using silver paste contact. The voltage criterion for the J_c measurement was 50 μV/cm. The thin films in the form of square shape having 10-mm length, 10-mm width and 1-mm thickness, and 200–250-nm thickness were used for the J_c measurements.

3 Results and discussion

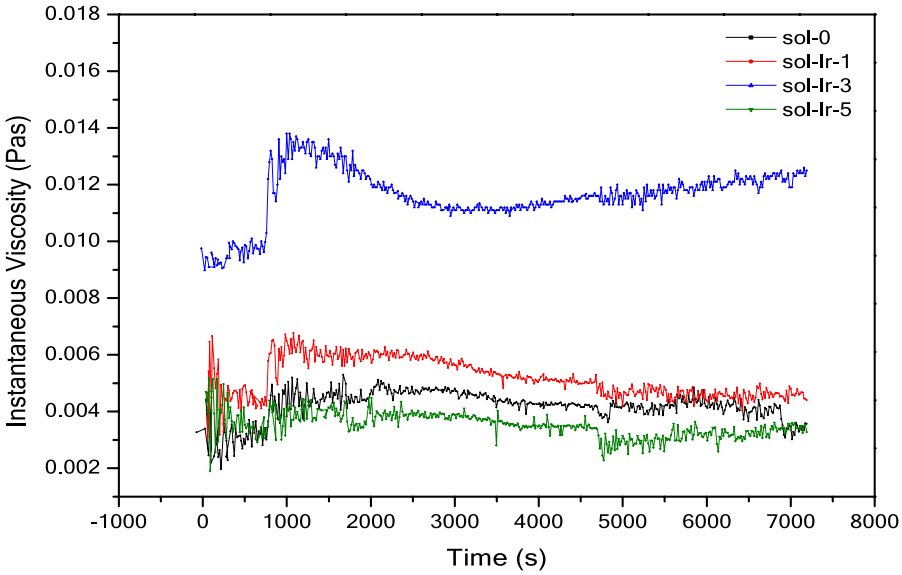
3.1 Solution characterization

3.1.1 Rheological properties

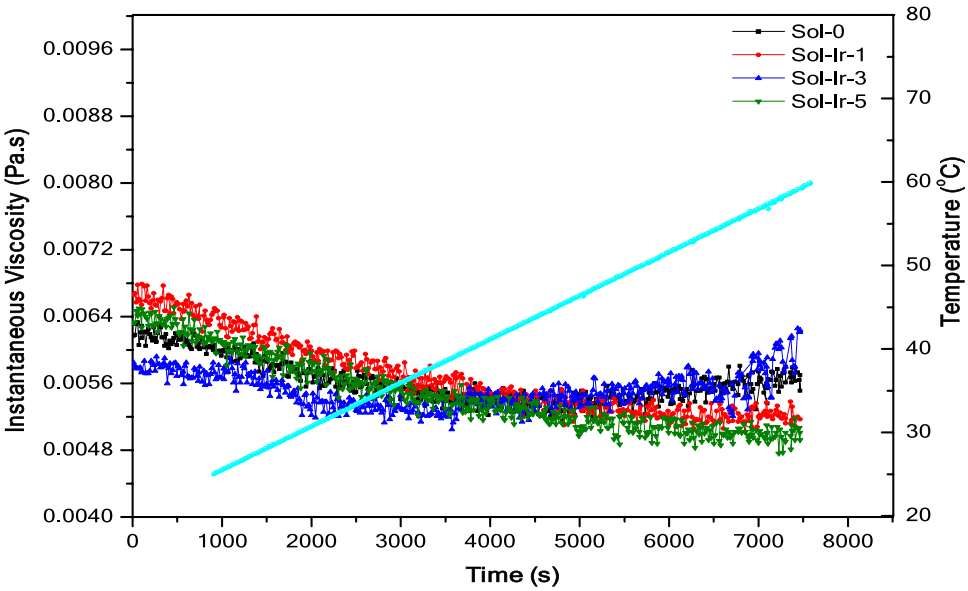
Rheological characterization of YBCO-based precursor solutions was performed to determine shear profile and temperature effect on their viscosity. The focus of attention here is mainly on the rheological properties in film production. The viscosity values of precursor solutions were determined at 25 °C in air at single shear mode under standard conditions and for 2 h with a constantly increasing shear rates [23].

Rheological properties of pure and Ir-doped YBCO precursor solutions are demonstrated in Figs. 5 and 6. Regarding the rheological properties of the precursor solutions, viscosity measurements of undoped/pure and BIO-doped YBCO solutions were carried out at room temperature and increasing shear rate, and at increasing temperature in the range of 25 °C and 60 °C and constant shear rate. Additionally, modulus measurements such as viscous and elastic modulus of the solutions were performed to anticipate their gel-point values.

Figure 5 denotes the variation of viscosity with increasing shear rate for Sol-0, Sol-Ir-1, Sol-Ir-3, and Sol-Ir-5 (Ir-added) solutions at 25 °C constant temperature. It was found that the viscosity value of solutions is nearly the same except Sol-Ir-3. However, the difference between the viscosity values is very small.



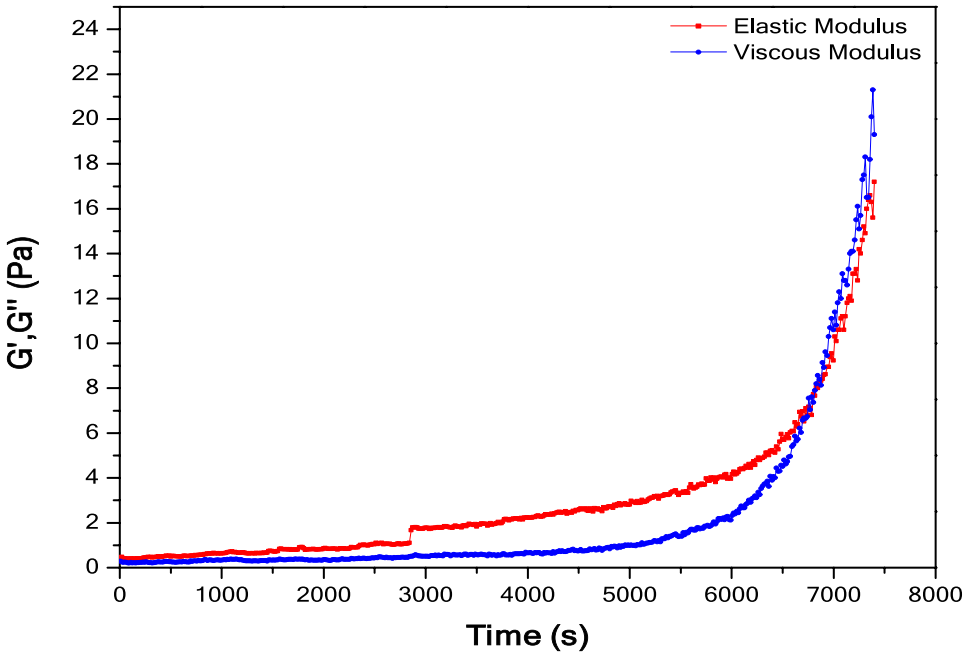
(a)



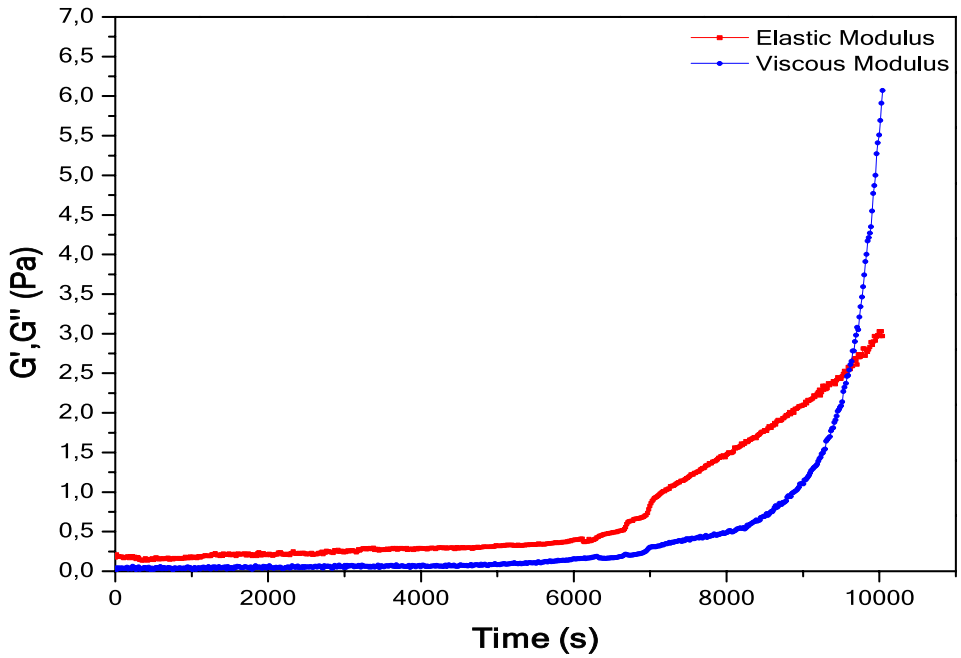
(b)

Fig. 5 Viscosity measurement of undoped and BIO-doped YBCO solutions **a** at room temperature and increasing shear rate and **b** at increasing temperature (25–60 °C) and constant shear rate

Therefore, it will not affect the film structure and thickness. The instantaneous viscosity versus temperature graph of undoped and Ir-added solutions are given in Fig. 5. Essentially, the same results were obtained for Ir-added solutions. At first, their viscosity decreases until 45 °C, and after that they reach a constant value. This is because solvent evaporated from precursor solutions. It is worth noting that the mean viscosity values are 4.19, 5.19, 11.63, and 3.54 mPa s for Sol-0, Sol-Ir-1, Sol-Ir-3, and Sol-Ir-5, respectively. The low viscosity of solutions signifies a high fluidity, indicating reduced resistance and easier flow. This condition typically reflects weaker intermolecular bonds or minimal friction between molecules at the molecular level within the solution. Consequently, solutions with low viscosity flow easily due to the presence of weak intermolecular bonds, approaching a contact angle close to 0°. This leads to the production of high-quality films, resulting in enhanced wetting and superior microstructures, as elaborated upon later.



(a)



(b)

Fig. 6 Modulus measurements of **a** pure and **b** 5 mol% BIO-doped YBCO solutions

As indicated in Table 2, the elastic modulus and viscous modulus of the solutions exhibited variations within the respective ranges of 2.00–13.00 Pa and 5.50–17.50 Pa. As explained elsewhere [24, 25], the elastic modulus represents the material's ability to regain its original shape after deformation when stress is removed, indicating its stiffness or elasticity. On the other hand, the viscous modulus reflects the material's

Table 2 Rheological and wettability properties of the solutions

Name of solution	Viscosity (mPa s)	Elastic modulus (Pa)	Viscous modulus (Pa)	Gelation time (s)	Contact angle (°)
Sol-0	4.19	13.00	17.50	6850	35.05
Sol-Ir-1	5.19	–	–	> 10,000	30.26
Sol-Ir-3	11.63	–	–	> 10,000	25.50
Sol-Ir-5	3.54	2.00	5.50	9800	26.70

resistance to flow or deformation over time, indicating its viscosity or fluidity. There are strong correlations between the elastic modulus and viscous modulus of solutions and coating quality. Generally, solutions with higher elastic moduli may lead to the formation of coatings with increased stiffness and resistance to deformation, thereby enhancing the durability and mechanical properties of the coating. Conversely, solutions with higher viscous moduli may result in coatings with improved flow and leveling characteristics, facilitating the attainment of smoother and more homogeneous coatings. Therefore, the measured elastic modulus and viscous modulus of the solutions are at the reasonable level.

Newtonian materials are characterized by a viscosity which may depend on the temperature but is independent of the shear rate (and shear stress). The viscosity of the non-Newtonian materials depends on the shear rate. Based on these viscosity results, undoped and doped YBCO solutions are Newtonian materials and their viscosity only depends on the processing temperature.

The gel-point values of undoped and Ir-added YBCO precursor solutions are shown in Fig. 6. Time of gelation can be determined for all solutions. Viscous and elastic moduli can be changed depending on time for our cases. The time necessary to reach the intersection depends on the viscous and elastic moduli oscillations. Thus, this intersection could be used to define the experimental gel point. It can be noticed from Fig. 6 that in spite of the fact that gelation time values of Sol-0 solution were 6850 s., that of Sol-Ir-5 was found to be 9800 s. which is very long period. Moreover, empirical observations reveal that the gelation durations of Sol-Ir-1 and Sol-Ir-3 solutions surpass the threshold of 10,000 s. An elevated gelation duration is deemed favorable as a precursor to coating procedures. Conversely, diminished gelation durations pose challenges to the coating process, precipitating spontaneous gelation of the solution during storage or quiescence. Consequently, an augmented gelation duration assumes paramount significance in the fabrication of superior-quality films. On the account of the fact that a very long gelation time is desirable during TFA-MOD processing in practical applications, these values are being made to harmonize solution preparation and to finalize well-textured, continuous superconducting thin films on STO substrates.

3.1.2 *Wettability behaviors*

Following the comprehensive determination of rheological properties, the assessment of the contact angle values for all YBCO-based precursor solutions on STO substrates was undertaken. As depicted in Fig. 7, the measurement of contact angles revealed noteworthy insights. Specifically, the average contact angle values were determined to be 35.05°, 30.26°, 25.50°, and 25.50° for the solutions such as Sol-0, Sol-Ir-1, Sol-Ir-3, and Sol-Ir-5, respectively. These findings signify favorable wettability characteristics, particularly for the coating solutions intended for STO substrates in the context of thin film production. As previously elucidated, there appears to be concordance between the rheological properties of solutions and wetting characteristics.

The observed contact angle values hold significance in influencing the quality of the surface film. Notably, the relatively low contact angles of the solutions indicate a propensity for good wetting behavior. In practical terms, a minute wetting angle approximating 0° is deemed desirable for real-world applications [26]. The implications of these results extend to the assurance of a uniformly homogeneous coverage on STO single-crystal substrates, crucial for the fabrication of high-quality thin films. This empirical evidence substantiates the efficacy of the coating solutions in achieving optimal wetting conditions on the substrate, underscoring the potential for enhanced surface film

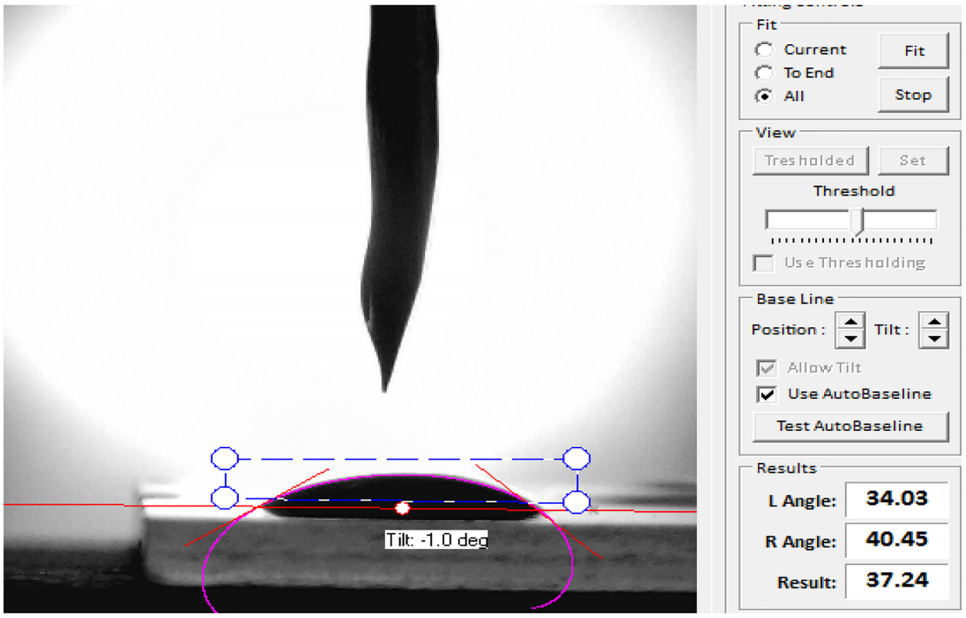


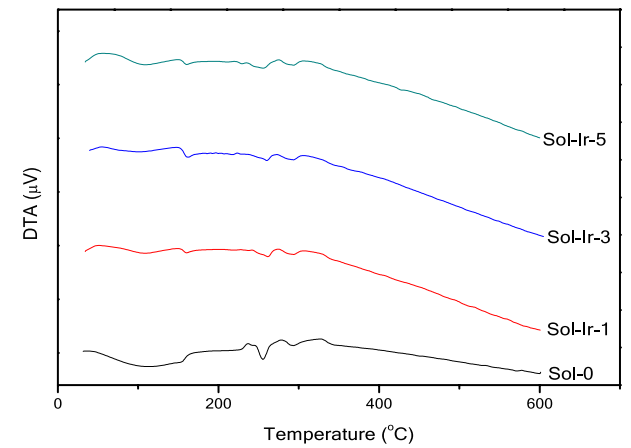
Fig. 7 Wettability of undoped/pure YBCO solution

quality in the production of YBCO-based superconducting thin films.

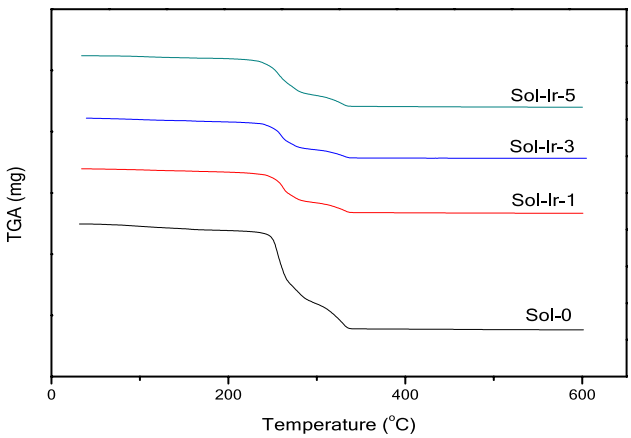
3.2 Material characterization

3.2.1 Thermal analysis

In the fabrication of homogeneous, crack-free, well-textured, and high-quality thin films, the pyrolysis stage plays a pivotal role. This critical phase involves the controlled heating of undoped and Ir-doped/added YBCO precursor solutions, where meticulous attention must be given to prevent detrimental effects on the thin film structures and superconducting properties. During the pyrolysis process, several intricate phenomena take place, including the vaporization of water and organic solvents, as well as the combustion of organic complexes. These chemical transformations hold the potential to adversely impact the overall quality and characteristics of the resulting thin films. Consequently, as a preemptive measure, prior to the heat treatment process, the undoped and Ir-doped/added YBCO precursor solutions undergo a drying step at 100 °C for 3 h in an air environment. To gain a comprehensive understanding of the thermal behavior and evolving chemical processes, DTA-TG analysis are employed. These analyses are conducted under a N_2 atmosphere, providing a controlled environment to examine the thermal transitions without the interference of external factors such as oxygen. Figure 8 illustrates the DTA and TG curves obtained from the



(a)



(b)

Fig. 8 **a** DTA and **b** TGA curves of undoped and BIO-doped YBCO xerogels dried at 100 °C for 3 h in air

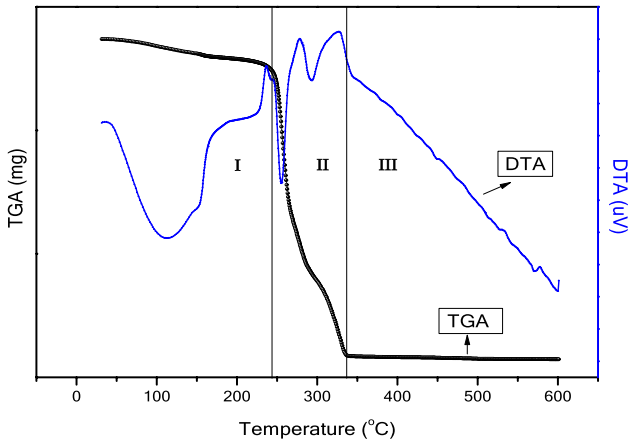


Fig. 9 DTA–TG curves of undoped YBCO xerogels dried at 100 °C for 3 h in air

YBCO-based xerogels, portraying the intricate thermal events and weight changes during the pyrolysis stage. This systematic approach, incorporating precise drying and analytical techniques, serves to optimize the fabrication process and enhance the overall quality of the resulting thin films, particularly with respect to their structural integrity and superconducting properties.

Llordes et al. [27] conducted a thorough analysis of the DTA and TG curves, discerning three distinct stages in the thermal evolution of the YBCO-based xerogels, as illustrated in Fig. 9. These stages are elucidated as follows: (a) Dehydration and evaporation (Stage I): In the initial stage (Stage I), the thermal profile is characterized by the simultaneous removal of water and the evaporation of organic solvents. This phase is critical in expelling volatile components, preparing the precursor materials for subsequent thermal transformations. (b) Thermolysis of coordinated solvents (Stage II): The subsequent stage (Stage II) involves the thermolysis of coordinated solvents. A notable and rapid weight loss is observed within the temperature range of 240–340 °C during this phase. This phenomenon signifies the breakdown of coordinated solvents within the precursor materials. (c) Thermooxidative decomposition of TFAs (Stage III): The final stage (Stage III) encompasses the thermooxidative decomposition of trifluoroacetate (TFA) salts. This thermal process contributes to the intricate chemical transformations, ultimately shaping the composition and characteristics of the thin films. Zhao et al. [28] provided additional insights by highlighting specific temperature thresholds. Below 240 °C, a gradual weight loss in the TGA curves is attributed to the release of organic solvents and water confined within the gel films. Concurrently, the DTA curves reveal exothermic reactions occurring between 240 and 340 °C, signifying the exothermic decomposition of TFA salts. This systematic delineation of distinct stages in the thermal evolution of YBCO-based xerogels, as illuminated by Llordes et al. [27] and Zhao et al. [28], provides a nuanced understanding of the intricate processes involved in the precursor material transformation during pyrolysis. Such insights are essential for tailoring and optimizing thin film fabrication processes to achieve desired structural integrity and superconducting properties.

Obradors et al. [18] summarized reactions in two step: firstly, calcination process will generate a homogeneous nanocrystalline film formed by CuO, Y_2O_3, and BaF_2, i.e., the decomposition reaction is

$$\begin{aligned} &Cu(TFA)_2 + Ba(TFA)_2 + Y(TFA)_3 \rightarrow CuO \\ &\quad + BaF_2 + Y_2O_3 + (CF_3CO)_2 + CO_2 \\ &\quad + CO + H_2O, \end{aligned} \tag{4}$$

In a second step, the metastable state created after the pyrolysis is heated to high temperatures (≈ 700–800 °C) under a controlled atmosphere and with a well-determined temperature ramp. It has been suggested that the YBCO phase formation proceeds following the reaction:

$$\begin{aligned} &2BaF_2 + 2CuO + 1/2Y_2Cu_2O_5 + 2H_2O(g) \\ &\quad \rightarrow YBa_2Cu_3O_{6+x} + 4HF(g) + (1/2 - x)O_2(g). \end{aligned} \tag{5}$$

3.2.2 *FTIR analysis*

The FTIR spectra of both undoped and BIO-doped YBCO precursor powders, subjected to a drying process at 100 °C in ambient air for 3 h, are presented in Fig. 10. Notably, a comprehensive examination of the FTIR spectra reveals an evident similarity between the undoped and BIO-doped solutions. Within the spectra, discernible bands at wavenumbers ranging from 2365 to 2345 cm^{-1} are attributed to the presence of carbon dioxide, originating both from atmospheric conditions and the decomposition of the gel matrix during the subsequent heat treatment process. This observation underscores the sensitivity of the FTIR technique in

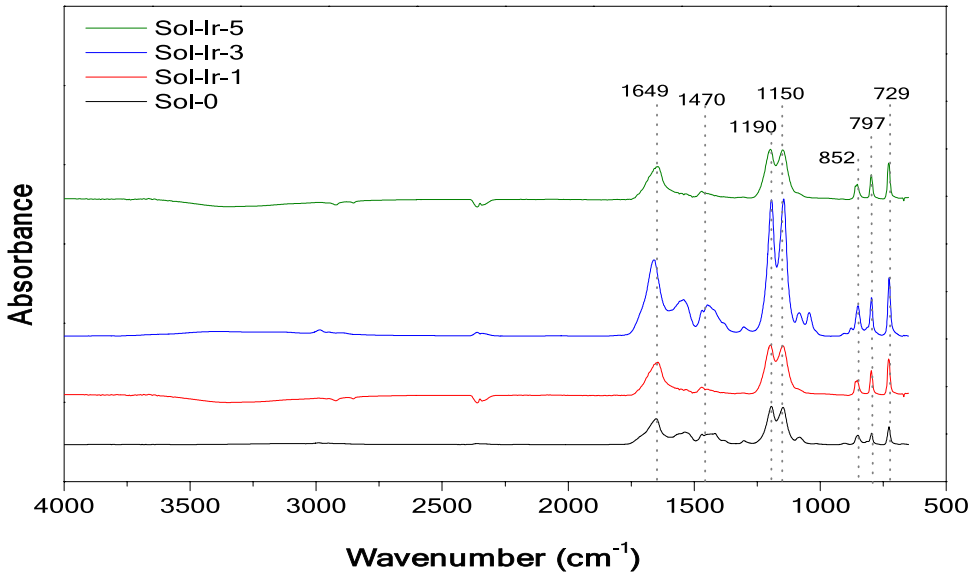


Fig. 10 FTIR spectra of undoped and BIO-doped YBCO powders dried at 100 °C for 3 h in air

capturing molecular interactions and transformations within the precursor powders.

Of particular interest is the observation that the acetate complexes within the precursor materials initiate decomposition at the relatively moderate temperature of 100 °C. This is elucidated by alterations in intensity and a shift toward lower wavenumbers in the corresponding bands. This phenomenon aligns with findings expounded in the research report by Thuy et al. [29], indicating the propensity of acetate complexes to undergo thermal decomposition at elevated temperatures.

This spectral analysis not only provides a qualitative insight into the chemical composition of the precursor powders but also underscores the influence of temperature on the structural dynamics of acetate complexes. Such detailed molecular investigations are imperative for a nuanced comprehension of the precursor's behavior, facilitating informed decisions in the optimization of heat treatment processes for the production of high-quality thin films.

3.2.3 *Phase analysis*

Figure 11 depicts the XRD patterns of both undoped and BIO-doped YBCO films (F-0, F(Ir-1), F(Ir-3), and F(Ir-5)), providing valuable insights into the crystalline structure of the films. Evidently, both undoped and BIO-doped films exhibit pronounced YBCO peaks when grown on STO substrates. The characteristic (00l) and (l00) reflections of the YBCO phase and STO substrate, respectively, are prominently featured in the XRD patterns. As evidenced in Ref. [30], the XRD analysis of BIO-doped YBCO thin films deposited on STO substrates, as illustrated in Fig. 11, manifests distinct diffraction peaks corresponding to the (001), (002), (003), (004), (005), (006), (007), and (008) planes of YBCO. These diffraction peaks, observed at 2θ angles of 8.50°, 15.20°, 22.90°, 30.03°, 39.50°, 47.03°, 55.40°, and 73.02°, respectively, signify the epitaxial growth along the c-axis or the texture axis. The crystallographic analysis indicates an orthorhombic structure akin to perovskite (JCPDS No. 40-0159). Specifically, the crystal lattice of YBCO films typically demonstrates a perovskite-like configuration characterized by alternating layers of Y, Ba, Cu, and O atoms. This arrangement is commonly described as a stratified assembly of CuO_2 planes interleaved with layers containing Y and Ba ions. YBCO, belonging to the class of high-temperature superconductors, underscores the pivotal role of its crystal structure in dictating its superconducting characteristics [31].

As elucidated in our earlier discussion on BIO-doped YBCO films, the discernible presence of these major peaks underscores the crystalline integrity and orientation of the YBCO films on the STO substrates. Notably, the predominant orientation along the c-axis, as evidenced by the (00l) reflections, signifies the highly textured nature of the YBCO films. This texturing is indicative of a superconducting phase,

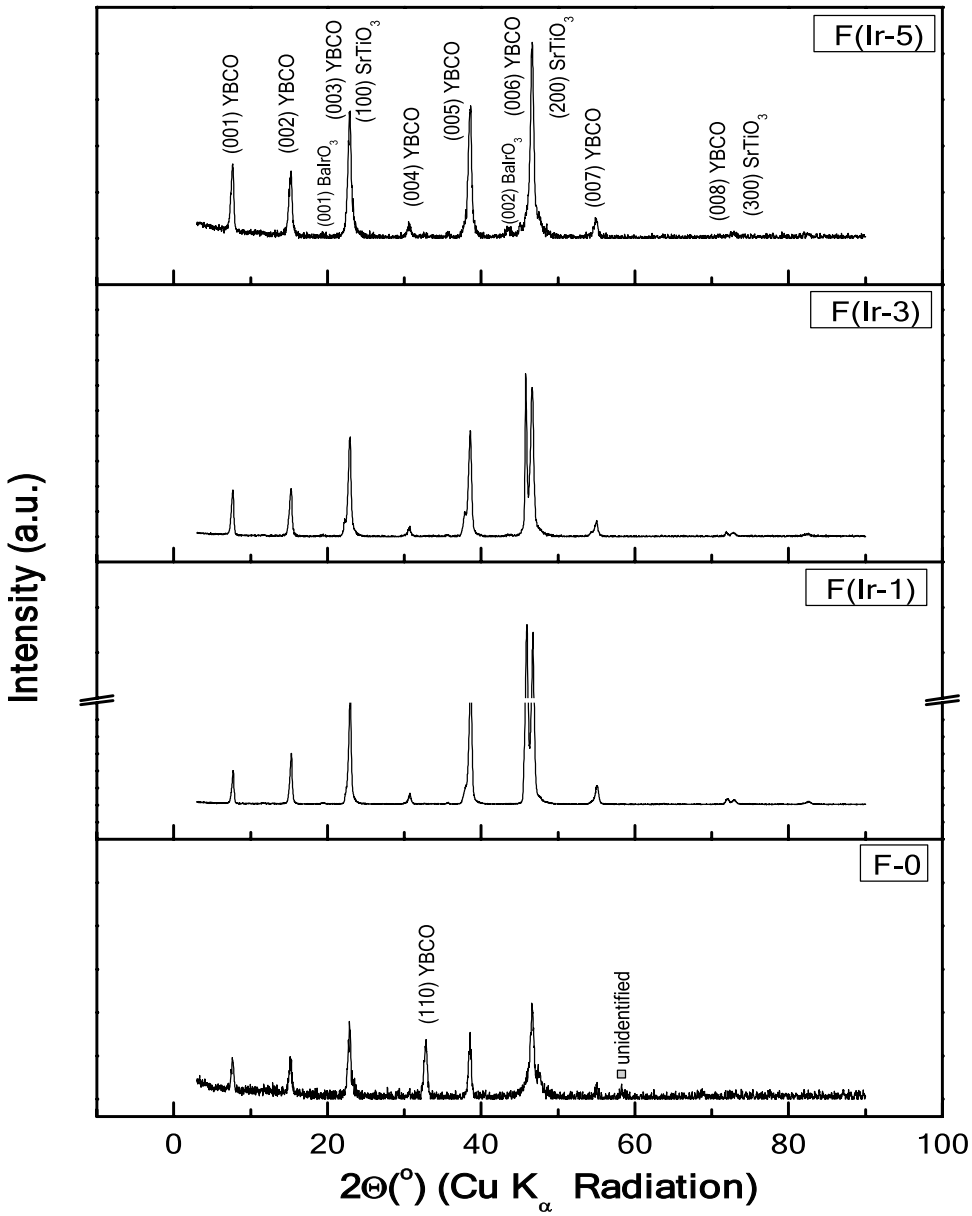


Fig. 11 X-ray θ–2θ scans of samples including undoped and BIO-doped YBCO with a CuK_{α} radiation. (YBCO JCPDS Card No: 040-0159, STO JCPDS Card No: 035-0734)

Table 3 Miller indices, 2θ angle, FWHM, texturing coefficient, average crystal sizes, and dislocation density values of YBCO-based films

Films	(hkl)	2θ (°)	FWHM (°)	TC	D (nm)	δ ($1/nm^3 \times 10^{-4}$)
0% BIO-YBCO	005	39.50	0.925	0.98	23.3	18.41
1% BIO-YBCO	005	39.55	0.910	1.00	26.5	14.23
3% BIO-YBCO	005	39.59	0.901	1.00	27.4	13.27
5% BIO-YBCO	005	39.62	0.885	1.00	28.5	12.32

thereby validating the desired superconducting properties of the films.

It is pertinent to note that, in the case of Ir-doped YBCO samples, an additional phase is observed in the form of BIO (002) peaks at $2\theta = 19.67°$. The identification of this secondary phase underscores the impact of Ir doping on the crystalline composition, introducing an additional crystalline component to the YBCO films. This observation holds

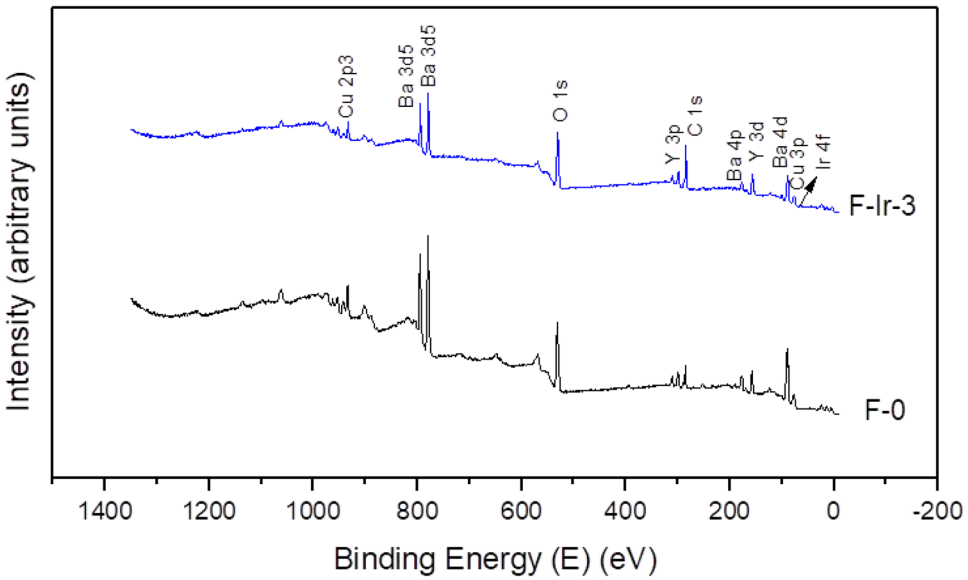


Fig. 12 XPS survey scans for F-0 and F(Ir-3) thin films

significance in the context of understanding the structural modifications induced by Ir doping and its potential implications on the superconducting properties of the films.

Table 3 presents Miller indices, diffraction angles, full width at half maximum (FWHM) values, texturing coefficients (*TC*), average crystal sizes (D), and dislocation density values for YBCO films doped with 0%, 1%, 3%, and 5% BIO on STO substrates. Utilizing the (005) Miller index, the interplanar distance and lattice constants (*a*, *b*, and *c*) were computed. The interplanar distance and lattice constants (*a*, *b*, and *c*) for both pure and BIO-doped YBCO films were determined using the (005) index, yielding values consistent with those depicted in the diffraction patterns. Based on the calculated interplanar distance, the lattice constants $a = 3.82$ Å, $b = 3.89$ Å, and $c = 11.67$ Å were ascertained. Notably, these lattice constants, particularly *a*, *b*, and *c*, align with those characteristics of a perovskite-like crystalline structure [32].

The texturing coefficient values of BIO-doped YBCO films were determined using Eq. 1 applied to XRD patterns, yielding values approximately within the range of 0.98 to 1.00. Remarkably, all films exhibited a notably high texturing coefficient, with the BIO-YBCO films displaying the highest coefficient of 1.00, indicative of a strong texture. However, it is noteworthy that the texturing coefficient of the 0% BIO-YBCO film slightly deviates at 0.98, albeit still within the range of other BIO-YBCO films. Despite this marginal difference, it is asserted that the 0% BIO-YBCO film can be considered to possess the highest texture. Additionally, the average crystallite sizes of the prepared samples were calculated utilizing Scherer's formula (Eq. 2) from the XRD patterns, crystal size of approximately 23.3 nm, 26.5 nm, 27.4 nm, and 28.5 nm for the 0%, 1%, 3%, and 5% BIO-doped YBCO films, respectively (for detailed values, refer to Table 3). Moreover, the dislocation density of the prepared films was computed using Eq. 3 from the XRD patterns, resulting in values approximately at 18.41×10^{-4} nm^{-3}, 14.23×10^{-4} nm^{-3}, 13.27×10^{-4} nm^{-3}, and 12.32×10^{-4} nm^{-3} for the 0%, 1%, 3%, and 5% BIO-doped YBCO films, respectively.

The XRD analysis presented in Fig. 11 offers a comprehensive overview of the crystallographic features of undoped and BiO-doped YBCO films, highlighting their orientation, phase purity, and the influence of Ir doping on the crystalline composition. Such detailed structural characterization is instrumental in correlating the observed material properties with the fabrication processes, ultimately guiding the optimization of thin film synthesis for enhanced superconducting performance.

3.2.4 XPS analysis

Figure 12 illustrates a comparative analysis of XPS survey scans pertaining to 0 and 3 mol% BIO-doped YBCO thin films deposited on STO single-crystal substrates. Notably, the discernible similarity in the overall chemical compositions of these films implies that dopant materials, specifically BIO, exhibit minimal

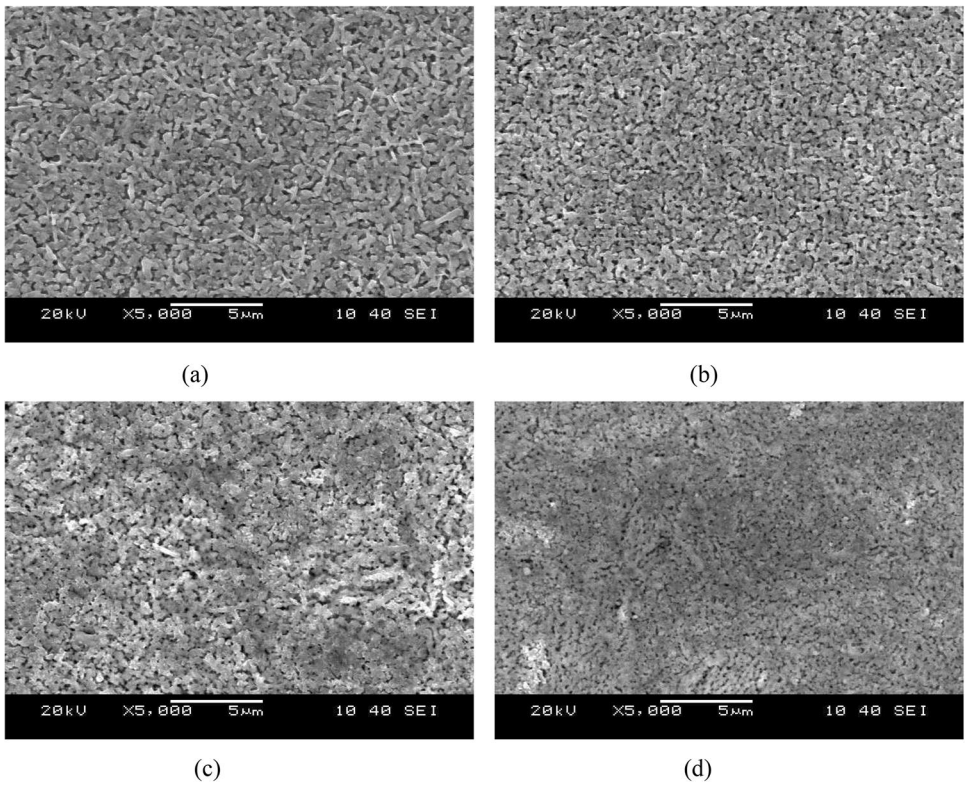


Fig. 13 SEM micrographs of pure and BIO-doped YBCO films on STO substrates, including **a** F-0, **b** F(Ir-1), **c** F(Ir-3), and **d** F(Ir-5) samples

influence on the overall chemistry of the YBCO samples, given their low concentration in the films.

The XPS survey scans reveal that the C 1 s peaks occur at 284 eV, with additional peaks at 291 eV attributed to the $–CF_3$ group and at 287.5 eV corresponding to –COOH. It is elucidated by Su et al. [33] that these components experience a reduction in intensity post-calcination, suggesting the decomposition of the fluoroacetate group during this thermal process. Furthermore, the absence of F 1s peaks is noteworthy.

In accordance with the findings, the C 1s peaks observed both before and after calcination can be ascribed to C–O–R entities and/or contaminants from the surrounding atmosphere, which are adsorbed during sample transfer. This underscores the nuanced chemical transformations and interactions occurring during the synthesis and processing stages of YBCO thin films. The detailed characterization elucidated in this analysis provides valuable insights into the chemical evolution and composition of these materials, contributing to a comprehensive understanding of their structural properties and potential applications in advanced materials science.

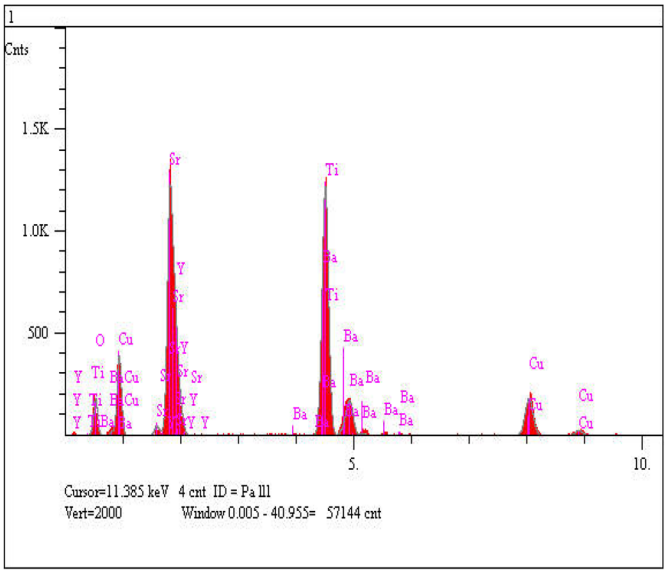
3.2.5 SEM–EDS analysis

Figure 13 presents an in-depth examination of the surface morphology of both undoped and BIO-doped YBCO thin films deposited on STO substrates. Notably, the visual assessment underscores the presence of consistently smooth and crack-free surfaces across all films, akin to the surfaces observed in BIO-doped samples. The significance of this observation is underscored by the imperative role of a smooth surface in optimizing the superconducting properties of these films. An essential characteristic in the evaluation of superconducting films is their c-axis orientation, and it is emphasized that these films predominantly exhibit such orientation, a crucial factor in enhancing their superconducting characteristics. SEM images reveal distinctive features in the form of needle-shaped crystal structures in 0 and 1 mol% doped YBCO films. Nevertheless, a notable transformation is evident in the case of 3 and 5 mol% BIO-doped YBCO films, where these needle-shaped particulates are conspicuously absent. An intriguing revelation from the SEM images is the discernible reduction in grain size in BIO-doped YBCO films compared to their undoped counterparts. This alteration in grain size is a pertinent observation,

Component	Mole Conc.	Conc.		
Y	5.082	9.098	wt.%	
Ba	2.210	6.110	wt.%	
Sr	20.246	35.722	wt.%	
O	37.259	12.004	wt.%	
Ti	25.273	24.360	wt.%	
Cu	9.930	12.706	wt.%	
	100.000	100.000	wt.%	Total

Elt.	Line	Intensity (c/s)	Error 2-sig	Conc		
O	Ka	15.44	0.786	12.004	wt.%	
Ti	Ka	160.55	2.534	24.360	wt.%	
Cu	Ka	31.33	1.119	12.706	wt.%	
Sr	La	111.57	2.112	35.722	wt.%	
Y	La	28.58	1.069	9.098	wt.%	
Ba	La	9.30	0.610	6.110	wt.%	
				100.000	wt.%	Total

kV	20.0
Takeoff Angle	35.0°
Elapsed Livetime	100.0

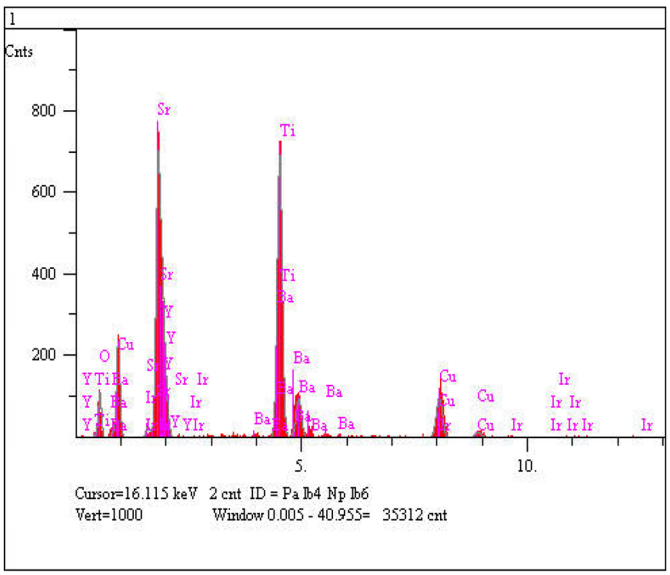


(a)

Component	Mole Conc.	Conc.		
Y	6.187	11.421	wt.%	
Ba	0.809	2.308	wt.%	
Sr	18.644	33.921	wt.%	
Ir	0.604	2.413	wt.%	
O	39.659	13.176	wt.%	
Ti	25.271	25.117	wt.%	
Cu	8.825	11.645	wt.%	
	100.000	100.000	wt.%	Total

Elt.	Line	Intensity (c/s)	Error 2-sig	Conc		
O	Ka	9.48	0.616	13.176	wt.%	
Ti	Ka	94.99	1.949	25.117	wt.%	
Cu	Ka	16.60	0.815	11.645	wt.%	
Sr	La	63.49	1.594	33.921	wt.%	
Y	La	21.43	0.926	11.421	wt.%	
Ba	La	2.01	0.283	2.308	wt.%	
Ir	La	0.56	0.149	2.413	wt.%	
				100.000	wt.%	Total

kV	20.0
Takeoff Angle	35.0°
Elapsed Livetime	100.0



(b)

Fig. 14 Elemental analysis and EDS spectra of **a** undoped and **b** 5 mol% BIO-doped YBCO films on STO substrates

as it holds potential implications for the film's structural and electrical properties. The absence of needle-shaped structures in higher BIO doping concentrations is indicative of the influence of the dopant on the film's morphology, potentially leading to enhanced structural homogeneity. In essence, the comprehensive analysis of surface morphology and crystal structures, elucidated through SEM imaging, provides valuable insights into the impact of BIO doping on the microstructural characteristics of YBCO thin films. These findings contribute to the nuanced understanding of the intricate interplay between dopant concentration and resulting material morphology, crucial for tailoring superconducting properties in advanced material design.

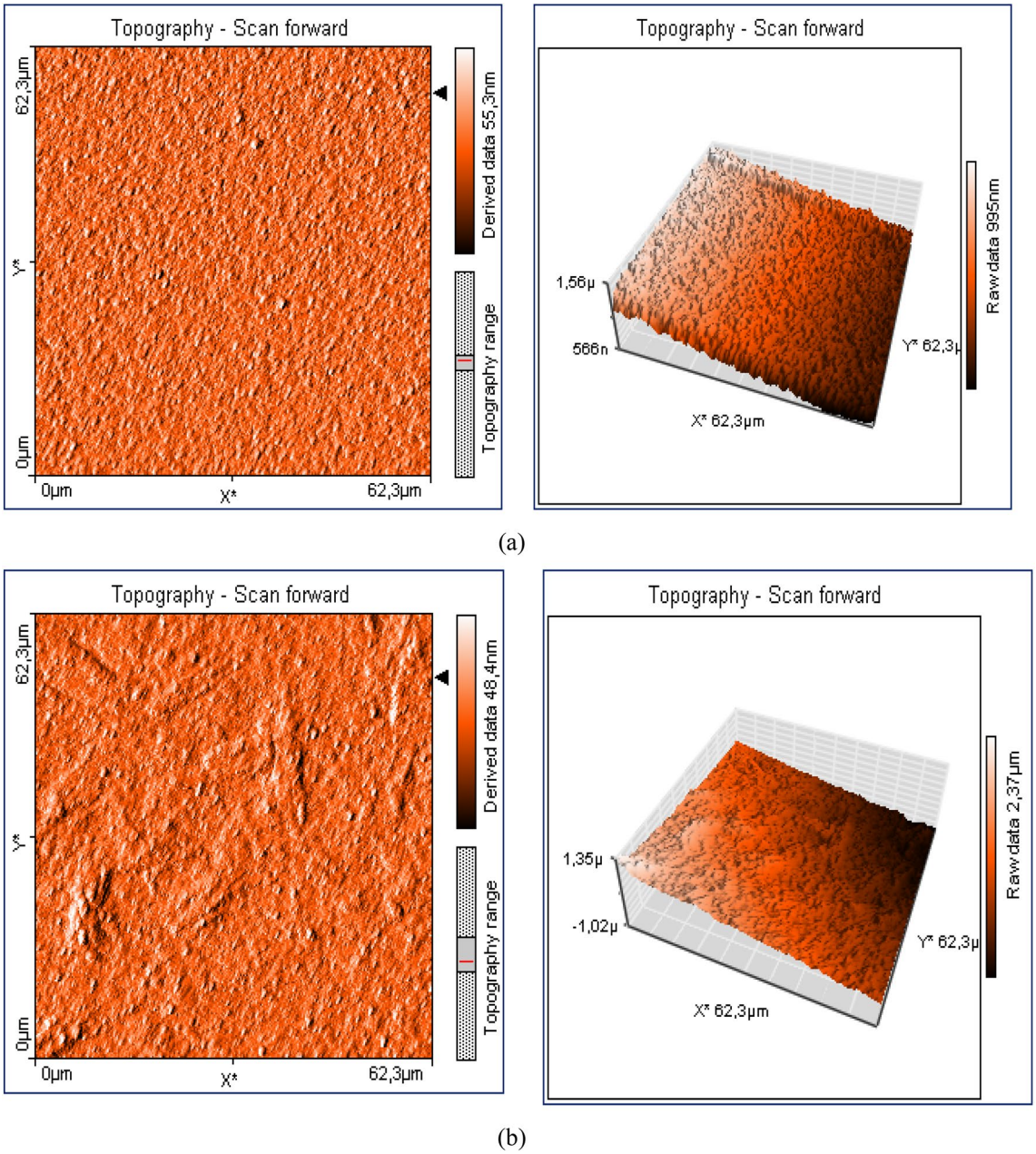


Fig. 15 AFM images of **a** F-0 and **b** F(Ir-3) thin films on STO substrates

Elemental analysis and EDS spectra of 0 and 5 mol% BIO-doped YBCO superconducting thin films deposited on STO single-crystal substrate with the aid of TFA-MOD technique are illustrated in Fig. 14 in detail. It can be seen clearly from the EDS spectrums that doped YBCO films contain Ir element. It was proved that perovskite BIO nanoparticles with (100) separately formed in YBCO structure by only adding Ir precursors. It makes possible to form $BaIrO_3$ perovskite structures by reacting Ba in YBCO structure with Ir element according to the following Eq. 6:

$$2Ba + 2Ir + 3O_2 \rightarrow 2BaIrO_3. \quad (6)$$

After these reactions, BIO nanostructures were easily formed as pinning centers in YBCO film on STO substrates. XRD results also supported them.

3.2.6 AFM analysis

The surface morphologies of YBCO-based samples are further scrutinized through AFM analysis, aimed at elucidating the surface roughness characteristics of superconducting thin films. Figure 15 presents 63.2 × 63.2 μm AFM 2D and 3D images, providing comprehensive visual representations of the surfaces of 0 and 3 mol% BIO-incorporated YBCO thin films deposited on STO substrates.

The evaluation of surface features is paramount in the realm of materials science and condensed matter physics. The utilization of AFM allows for a high-resolution examination, enabling the determination of surface roughness values. The depicted AFM images serve as indispensable tools for elucidating the topographical intricacies of the examined thin films.

Within this analytical framework, the average surface roughness (S_a) emerges as a critical parameter for quantifying the irregularities on the thin film surfaces. The obtained S_a values, 5.23 nm for the undoped sample denoted as F-0 and 6.73 nm for the 3 mol% BIO-added sample denoted as F(Ir-3), provide quantitative insights into the comparative roughness characteristics. The observed disparities in surface roughness values could potentially be attributed to the influence of BIO doping, thereby influencing the structural and morphological attributes of the YBCO thin films.

In a broad context, the assessment of surface roughness is a pivotal aspect in material characterization, particularly in solution-based techniques where it typically falls within the range of 40–100 nm. However, within the scope of our investigation, the determined surface roughness values markedly surpass this conventional range. It can be asserted that the surface quality of YBCO-based films has undergone a considerable enhancement. In the realm of materials science and thin film technology, the discernment of surface quality assumes paramount importance due to its profound implications for the functional and structural attributes of materials. In the present study, the observed surface roughness values significantly outperform the established benchmarks associated with solution-based methodologies. This noteworthy deviation underscores the efficacy of the employed fabrication techniques and underscores the heightened quality of the YBCO-based films under scrutiny. The discernible improvement in surface quality is indicative of the successful optimization of fabrication parameters and deposition processes. This advancement is likely attributable to the meticulous control and manipulation of experimental variables, including precursor concentrations, deposition temperatures, and substrate interactions. Such refined control mechanisms are instrumental in steering the morphology and topographical features of thin films toward enhanced quality.

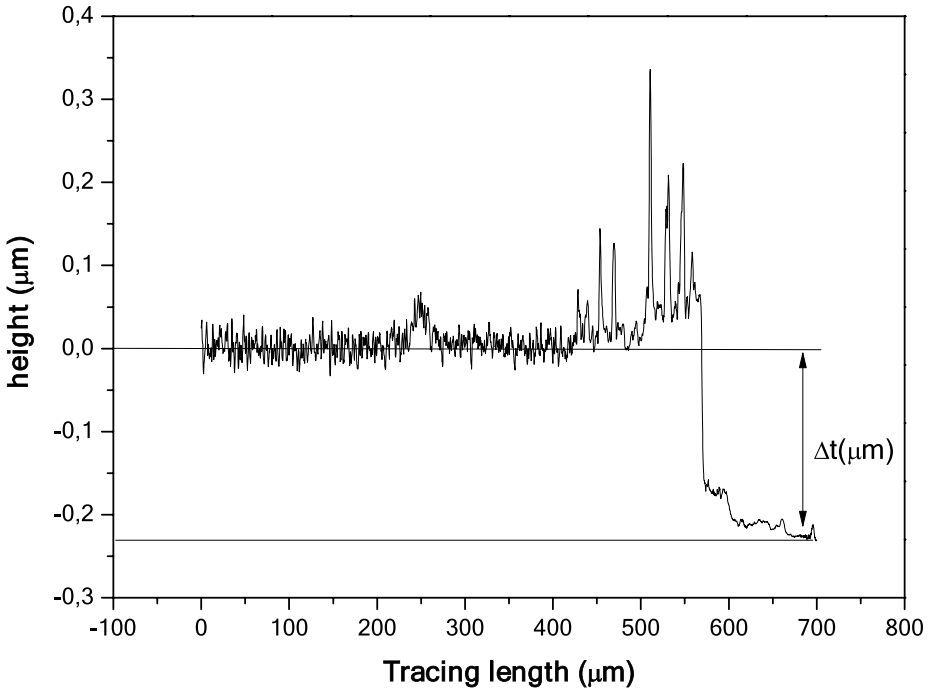
3.2.7 Film thickness

The elucidation of thin film thickness for F-0 and F(Ir-3) is graphically presented in Fig. 16a and b, respectively. The quantitative assessment reveals an average film thickness of approximately 240 nm, a parameter of substantial import in the domain of thin film science. The comparative analysis between undoped (F-0) and doped (F(Ir-3)) YBCO films is noteworthy for its revelation of nearly identical thickness values. This observation underscores a noteworthy consistency in the film deposition process, irrespective of the incorporation of doping material. The apparent lack of discernible variation in thickness between undoped and doped films suggests a robust and controlled deposition mechanism, wherein the doping material does not exert a significant influence on the final thickness of the YBCO films.

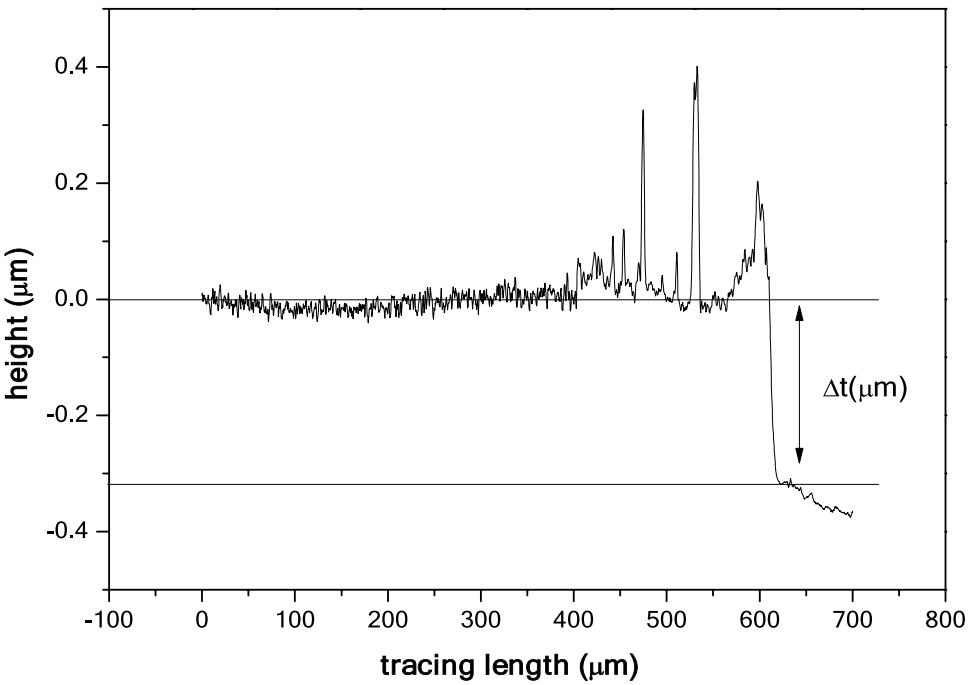
In the parlance of materials science and thin film technology, the uniformity in film thickness is indicative of precision and control in the experimental methodology. The negligible impact of doping material on thickness implies that the introduced dopant does not appreciably alter the deposition kinetics or contribute to variations in film growth. This finding holds significance for applications where precise control over film thickness is paramount, as it suggests that doping, in this context, is not a determinant factor influencing this crucial parameter.

3.2.8 Superconducting properties

Figure 17 illustrates the resistivity shift with temperature for both undoped and BIO-doped YBCO thin films. The undoped YBCO thin film exhibits a high critical temperature (T_c) value of 92 K but displays a significant transition width (ΔT_c), indicative of a lack



(a)



(b)

Fig. 16 Determination of film thickness for **a** F-0 and **b** F(Ir-3) thin films on STO substrates

of sharp transition. The broad ΔT_c serves as a metric for assessing the quality and homogeneity of the samples, with higher ΔT_c values suggesting inferior superconducting properties attributable to the presence of secondary phases in the undoped YBCO film. In contrast, BIO-doped YBCO thin films demonstrate

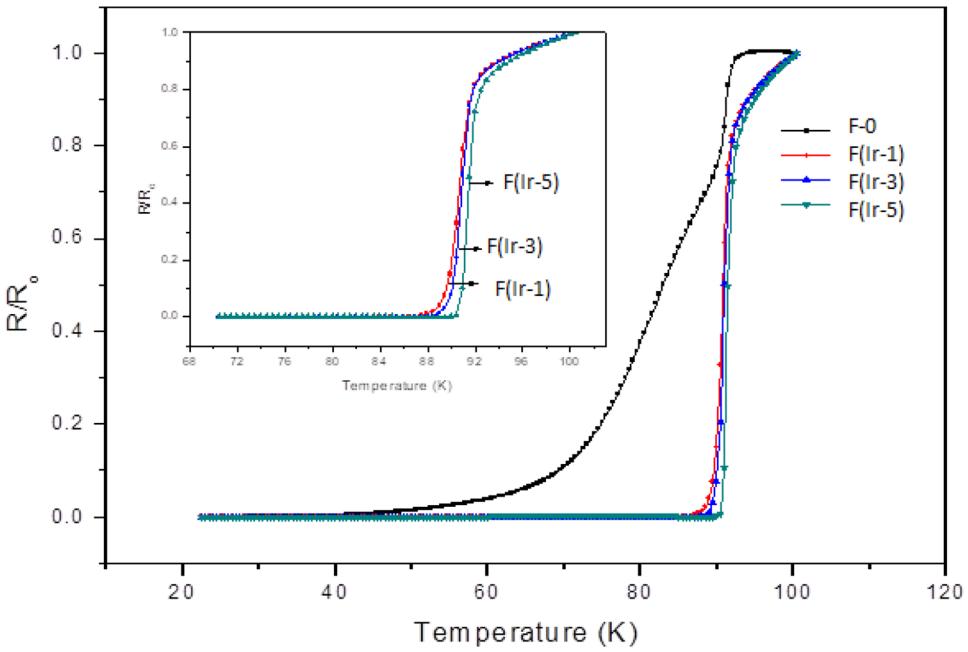


Fig. 17 Resistance vs. temperature graph of BIO-doped YBCO thin films

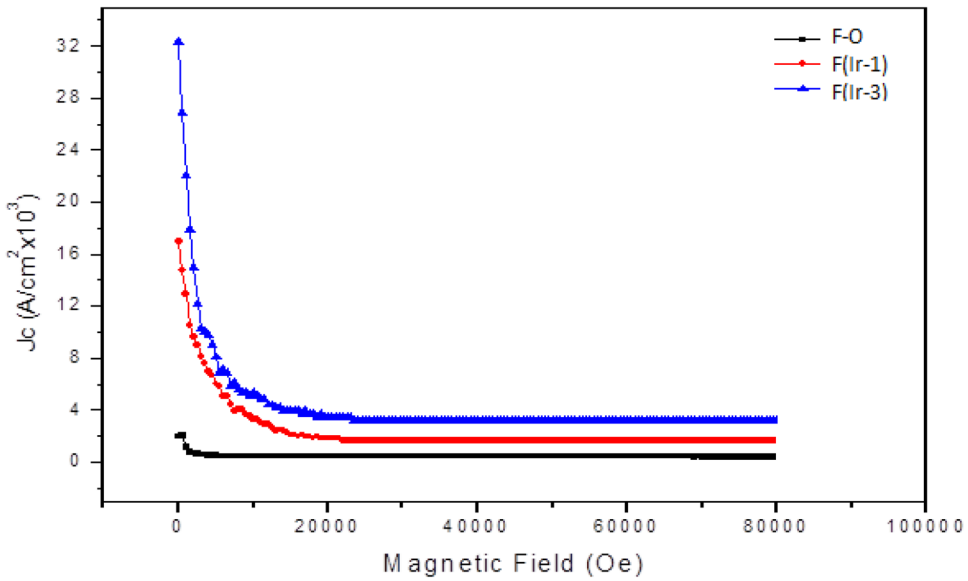


Fig. 18 Critical current density vs. magnetic field graph of BIO-doped YBCO thin films

a high T_c (>91 K) and a reduced ΔT_c (approximately 1.5 K), signifying improved homogeneity and quality. Notably, all Ir-added films exhibit sharp transitions, as evidenced in Fig. 17. The inset graph accentuates the impact of BIO, revealing that an increase in BIO concentration from 1 to 5 mol% correlates with an elevation in T_c value and a concurrent decrease in ΔT_c. The film containing 5 mol% Ir displays the lowest ΔT_c, suggesting enhanced superconducting properties.

Figure 18 presents the critical current density (J_c) versus magnetic field graph for both undoped and Ir-added films. Undoped YBCO film exhibits a suboptimal J_c value under zero magnetic field, mirroring its unfavorable T_c performance owing to the presence of secondary phases. However, as Ir concentration increases, J_c values improve under zero magnetic field, reaching 3.2×10^4 A/cm^2 with a 3 mol% Ir addition. Notably, the critical current density values decline rapidly for all YBCO films as the magnetic

field increases from 0 to 9 T. Comparatively, the attained J_c values appear relatively low when benchmarked against existing literature. Hänisch et al. [34] conducted a study involving BIO precipitates on YBCO thin films using the PLD technique, investigating its pinning properties. In their work, transport measurements were carried out using bridges on thin films, resulting in a notably higher value of 3×10^6 A/cm^2.

4 Conclusion and future plans

In summary, production and characterization of undoped and BIO-doped YBCO superconductor thin films on STO substrates were investigated by using TFA-MOD technique. Acetate base precursor chemicals were used to produce thin film.

Firstly, solution characterization was performed. Contact angle and rheological properties of undoped and doped precursor solutions were investigated. Contact angle value of the undoped YBCO solution on STO substrate was measured as 35.05°, and this value lower than 90°; therefore, these solutions can wet the single-crystal substrates. Rheological characterization was performed to determine shear profile and effect of temperature on viscosity. For all solutions, at first viscosity value decreases with increasing temperature, but then they reach a constant value. Under increasing temperature conditions, undoped and doped YBCO solutions are Newtonian materials and their viscosity only depends on the temperature.

To determine heat treatment regime, DTA-TG characterization was performed. At lower temperature (< 240 °C), organic solvent and water confined to gel films run out, which was clarified from a slow weight loss in TGA curves. The TFA salts decompose which are exothermic reactions at temperature between 240 and 340 °C. At the same time, fast weight losses between 240 and 340 °C can be seen from all the TGA curves.

The phase structure of YBCO thin films was determined by XRD. In XRD patterns, generally the major peaks correspond to the (00l) reflections of the YBCO phases and (100) STO substrate, which indicates that the films have a strong c-axis texture. Unfortunately, undoped YBCO thin film includes some secondary phase at the same fabrication conditions.

In order to measure the chemical or electronic state of surface elements, XPS was used. The overall chemical compositions of all the films look very similar and it should be noted that doping does not affect the overall chemistry of the films.

SEM and AFM were used to identify surface morphologies of YBCO thin films on single-crystal STO substrates. In general, the surface morphologies of all samples have continuous, flat, and crack-free surfaces. However, some a-axis-oriented grains is observed for F-0. BIO-doped YBCO films present a denser surface structure compared with the undoped YBCO films. Average film thickness value of YBCO samples is determined nearly 240 nm.

The critical transition temperature, critical current density, and critical magnetic field of samples were determined by using PPMS device. Standard four-probe technique with silver paste contacts was used. Undoped YBCO film shows bad superconducting properties due to the secondary phases. Generally speaking, high T_c and low ΔT_c values were obtained for all Ir-added YBCO thin films. J_c value also increased with BIO nanoparticle addition under magnetic field. The pinning effect was observed with Ir addition. BIO nanoparticle addition has also affected the YBCO superconducting properties.

It is recommended that acetate base precursor chemicals are more expensive than commercially available YBCO powder. Therefore to produce cheaper films, BIO-doped precursor solutions can be prepared by using YBCO powder. To decrease a- or b-axis grains and increase surface morphology of final thin films, barium poor precursor solutions can be prepared. Determination of superconducting properties of thin films is very important issue. Standard four-probe method with silver paste contact does not give accurate results. To reach high critical current density at high magnetic fields, bridges have to be patterned on films by using lithography devices and very small areas have to be used.

Acknowledgements

This work was carried out at Dokuz Eylul University, Department of Metallurgical and Materials Engineering and Center for Electronic Material Fabrication (Izmir, Turkiye). We also greatfully acknowledge the financial assistance provided by the Scientific and Technological Research Council of Turkiye (TUBITAK), under project number 109M054.

Author contributions

All authors contributed to the study conception and design. All authors read and approved the final manuscript.

Funding

Open access funding provided by the Scientific and Technological Research Council of Türkiye (TÜBİTAK). This research did not receive any specific grant from funding agencies in the public, commercial, or not-for-profit sectors.

Data availability

Data sharing is not applicable to this article as no datasheets were generated and analyzed during the current study.

Declarations

Conflict of interest The authors declare that they have no known competing financial interests or personal relationships that could have appeared to influence the work reported in this paper.

Consent to participate Consent was obtained from all authors prior to, during, and now for submission.

Consent to publication All the authors agree to publication of the manuscript in its current form.

Open Access This article is licensed under a Creative Commons Attribution 4.0 International License, which permits use, sharing, adaptation, distribution and reproduction in any medium or format, as long as you give appropriate credit to the original author(s) and the source, provide a link to the Creative Commons licence, and indicate if changes were made. The images or other third party material in this article are included in the article's Creative Commons licence, unless indicated otherwise in a credit line to the material. If material is not included in the article's Creative Commons licence and your intended use is not permitted by statutory regulation or exceeds the permitted use, you will need to obtain permission directly from the copyright holder. To view a copy of this licence, visit http://creativecommons.org/licenses/by/4.0/.

References

1. A.K. Jha, N. Khare, J. Magn. Magn. Mater. (2010). https://doi.org/10.1016/j.jmmm.2010.04.002
2. X. Zhou, J. Chen, Z. Liu, C. Cai, Ceram. Int. (2024). https://doi.org/10.1016/j.ceramint.2023.11.398
3. I. Mukherjee, P. Mandal, A.K. Ghosh, Physics C (2024). https://doi.org/10.1016/j.physc.2023.1354410
4. K. Knoth, S. Engel, C. Apetrii, M. Falter, B. Schlobach, R. Hühne, S. Oswald, L. Schultz, B. Holzapfel, Curr. Opin. (2006). https://doi.org/10.1016/j.cossms.2007.07.001
5. C. Zhang, X. Du, H. Zhang, Physics C (2020). https://doi.org/10.1016/j.physc.2020.1353737
6. W.T. Wang, G. Li, M.H. Pu, R.P. Sun, H.M. Zhou, Y. Zhang, H. Zhang, Y. Yang, C.H. Cheng, Y. Zhao, Physics C (2008). https://doi.org/10.1016/j.physc.2008.05.067
7. K. Nakaoka, J. Matsuda, Y. Kitoh, T. Goto, Y. Yamada, T. Izumi, Y. Shiohara, Physics C (2007). https://doi.org/10.1016/j.physc.2007.04.264
8. K. Nakaoka, M. Yoshizumi, Y. Usui, T. Izumi, Y. Shiohara, Phys. Proc. (2014). https://doi.org/10.1016/j.phpro.2014.09.022
9. Y. Miyanaga, R. Teranishi, K. Yamada, N. Mori, M. Mukaida, T. Kiss, M. Inoue, K. Nakaoka, M. Yoshizumi, T. Izumi, Y. Shiohara, M. Nanba, S. Awaji, K. Watanabe, Physics C (2009). https://doi.org/10.1016/j.physc.2009.05.049
10. T. Araki, I. Hirabayashi, Supercond. Sci. Technol. (2003). https://doi.org/10.1088/0953-2048/16/11/R01
11. M. Bektas, I. Birlik, A.N. Ozcivan, E. Celik, AKU J. Sci. Eng. (2014). https://fenbildergi.aku.edu.tr/14OS/025716(99-102).pdf
12. S. Engel, T. Thersleff, R. Hühne, L. Schultz, B. Holzapfel, Appl. Phys. Lett. (2007). https://doi.org/10.1063/1.2711761
13. M.P. Delamare, M. Hervieu, G. Desgardin, B. Raveau, Mater. Sci. Eng. B (1994). https://doi.org/10.1016/0921-5107(94)90150-3
14. F. Ding, H. Gu, T. Zhang, H. Wang, F. Qu, S. Dai, X. Peng, J. Cao, J. Alloys Compd. (2012). https://doi.org/10.1016/j.jallcom.2011.10.035
15. T. Aytug, M. Paranthaman, E. Specht, Y. Zhang, K. Kim, Y.L. Zuev, C. Cantoni, A. Goyal, D.K. Christen, V.A. Maroni, Y. Chen, V. Selvamanickam, Supercond. Sci.

Technol. (2010). https://doi.org/10.1088/0953-2048/23/1/014005
16. I. Birlik, M. Erbe, T. Freudenberg, E. Celik, L. Schultz, B. Holzapfel, J. Phys, Conf. Ser. (2010). https://doi.org/10.1088/1742-6596/234/1/012004
17. N. Roma, S. Morlens, S. Ricart, K. Zalamova, J. Moreto, A. Pomar, Supercond. Sci. Technol. (2006). https://doi.org/10.1088/0953-2048/19/6/019
18. X. Obradors, T. Puig, A. Pomar, N. Mestres, F. Sandiumenge, S. Pinol, O. Castano, A. Cavallaro, A. Palau, J.C. Gonzalez, M. Coll, J. Gazquez, Physics C (2004). https://doi.org/10.1016/j.physc.2004.03.160
19. A. Crisan, V.S. Dang, P. Mikheenko, Physics C (2017). https://doi.org/10.1016/j.physc.2016.06.011
20. S. Aksoy, Physical characterization of nano-structured metal oxide films obtained by sol gel spin coating method, PhD Thesis, Anadolu University, Institute of Science and Technology, Eskisehir (2017)
21. C. Kittel, *Introduction to Solid State Physics*, 8th edn. (Wiley, New York, 2005)
22. E. Kaelble, *Handbook of X-Rays for Diffraction, Emission, Absorption and Microscopy*, 6th edn. (McGraw-Hill, New York, 1967)
23. J.W. Ekin, Experimental techniques for low temperature measurements: cryostat design, material properties and superconductor critical-current testing. Oxf. Univ. Press (2006). https://doi.org/10.1063/1.2743130
24. S. Fundarò, G. Salti, D. Malvin, H. Malgapo, S. Innocenti, Int. J. Mol. Sci. (2022). https://doi.org/10.3390/ijms231810518
25. Y. Wang, Z. Li, L. Tian, Z. Shang, Ultrason. Sonochem. (2023). https://doi.org/10.1016/j.ultsonch.2023.106290
26. T. Huhtamäki, X. Tian, J. Korhonen, R.H.A. Ras, Nat. Protoc. (2018). https://doi.org/10.1038/s41596-018-0003-z
27. A. Llordes, K. Zalamova, S. Ricart, A. Palau, A. Pomar, T. Puig, A. Hardy, M.K. Van Bael, X. Obradors, Chem. Mater. (2010). https://doi.org/10.1021/cm903080k
28. B. Zhao, Z.Y. Sun, K. Shi, J. Yang, Y.P. Sun, Z.H. Han, Physics C (2003). https://doi.org/10.1016/S0921-4534(02)02195-0
29. T.T. Thuy, S. Hoste, G.G. Herman, K. De Buysser, P. Lommens, J. Feys, D. Vandeput, I. Van Driessche, Sol-Gel Sci. Technol. (2009). https://doi.org/10.1007/s10971-009-1987-1
30. J. Du, S. Gnanarajan, A. Bendavid, Physics C (2004). https://doi.org/10.1016/j.physc.2003.07.005
31. L.H. Jin, S.N. Zhang, Z.M. Yu, C.S. Li, J.Q. Feng, A. Sulpice, Y. Wang, P.X. Zhang, Mater. Chem. Phys. (2015). https://doi.org/10.1016/j.matchemphys.2014.10.005
32. M.T. Yurtcan, O. Simsek, O. Bayram, M. Ertugrul, East. Anatol. J. Sci. (2017). https://dergipark.org.tr/tr/download/article-file/376862
33. J. Su, P. Joshi, V. Chintamaneni, M. Mukhopadhyay, Supercond. Sci. Technol. (2005). https://doi.org/10.1088/0953-2048/18/11/015
34. J. Hänisch, C. Cai, R. Hühne, L. Schultz, B. Holzapfel, Appl. Phys. Lett. (2005). https://doi.org/10.1063/1.1894599

Publisher's Note Springer Nature remains neutral with regard to jurisdictional claims in published maps and institutional affiliations.